THE EFFECTS OF NOISE ON NONLINEAR SYSTEMS NEAR CRISIS

by

John Curtis Sommerer

Dissertation submitted to the Faculty of the Graduate School
of the University of Maryland in partial fulfillment
of the requirements for the degree of
Doctor of Philosophy
1991

Advisory Committee:

Professor Edward Ott, Chairman and Advisor
Professor James A. Yorke
Professor Thomas M. Antonsen, Jr.
Associate Professor Celso Grebogi
Assistant Professor Frederick N. Skiff
William L. Ditto (U.S. Naval Surface Warfare Center)

REPORT DOCUMENTATION PAGE

AFRL-SR-BL-TR-98-

0731

1. AGENCY USE ONLY (Leave Blank)	2. REPORT DATE	3. REPORT TYPE AND DATES COVERED
	1991	Final

4. TITLE AND SUBTITLE
The Effects of Noise on Nonlinear Systems Near Crisis

5. FUNDING NUMBERS

6. AUTHORS
John Curtis Sommerer

7. PERFORMING ORGANIZATION NAME(S) AND ADDRESS(ES)
University of Maryland

8. PERFORMING ORGANIZATION REPORT NUMBER

9. SPONSORING/MONITORING AGENCY NAME(S) AND ADDRESS(ES)
AFOSR/NI
4040 Fairfax Dr, Suite 500
Arlington, VA 22203-1613

10. SPONSORING/MONITORING AGENCY REPORT NUMBER

11. SUPPLEMENTARY NOTES

12a. DISTRIBUTION AVAILABILITY STATEMENT
Approved for Public Release

12b. DISTRIBUTION CODE

13. ABSTRACT *(Maximum 200 words)*
See attachment

14. SUBJECT TERMS

15. NUMBER OF PAGES

16. PRICE CODE

17. SECURITY CLASSIFICATION OF REPORT	18. SECURITY CLASSIFICATION OF THIS PAGE	19. SECURITY CLASSIFICATION OF ABSTRACT	20. LIMITATION OF ABSTRACT
Unclassified	Unclassified	Unclassified	UL

ABSTRACT

Title of Dissertation: **THE EFFECTS OF NOISE ON NONLINEAR SYSTEMS NEAR CRISIS**

John Curtis Sommerer, Doctor of Philosophy, 1991

Dissertation directed by Professor Edward Ott, Ph. D.,
Department of Physics and Astronomy, and
Department of Electrical Engineering

We consider the influence of random noise on low-dimensional, nonlinear dynamical systems with parameters near values leading to a crisis in the absence of noise. In a crisis, one of several characteristic changes in a chaotic attractor takes place as a system parameter p passes through its crisis value p_c. For each type of change, there is a characteristic temporal behavior of orbits after the crisis ($p>p_c$ by convention), with a characteristic time scale τ. For an important class of deterministic systems, the dependence of τ on p is $\tau\sim(p-p_c)^{-\gamma}$ for p slightly greater than p_c. When noise is added to a system with $p<p_c$, orbits can exhibit the same sorts of characteristic temporal behavior as in the deterministic case for $p>p_c$ (a noise-induced crisis). Our main result is that for systems whose characteristic times scale as above in the zero-noise limit, the characteristic time in the noisy case scales as $\tau\sim\sigma^{-\gamma}g[(p_c-p)/\sigma]$, where σ is the characteristic strength of the noise, $g(\bullet)$ is a non-universal function depending on the system and noise, and γ is the critical exponent of the corresponding deterministic crisis. Illustrative numerical examples are given for two-dimensional maps and a three-dimensional flow. In addition, the relevance of the noise scaling law to experimental situations is discussed.

We investigate experimentally the scaling of the average time τ between intermittent, noise-induced bursts for a chaotic mechanical system near a crisis. The system studied is a periodically driven, variable-noise, magnetoelastic ribbon. We determine γ for the low-noise ("deterministic") system, then add noise and observe that the scaling for τ is as predicted.

Dedicated to
Suzette Sommerer

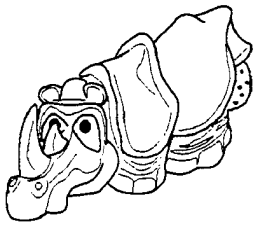

ACKNOWLEDGMENTS

I would like to acknowledge the guidance of Edward Ott and Celso Grebogi, who suggested that I work on the problem of noise-induced crises. It has been a privilege to work with them. I also thank fellow graduate student Mingzhou Ding for "showing me the ropes."

At the Applied Physics Laboratory, thanks to Julie Bowen for a strategically timed impetus, to Allan Bjerkaas for ignoring my total lack of preparation for graduate study in physics, and to Barry Raff for the peace of mind resulting from a known safe haven.

At the Naval Surface Warfare Center, my thanks go to the Magnetics Group in general and to Bill Ditto and Mark Spano in particular for their hospitality and generosity in offering me the use of their facilities.

Thanks also to the University of Maryland Graduate School for financial support through a University Fellowship, and to the U. S. Air Force Office of Scientific Research for financial support through a National Defense Science and Engineering Graduate Fellowship. The numerical experiments were carried out using the facilities of the National Energy Research Supercomputer Center.

Most of all, I thank Suzette Sommerer for her continuing support.

CONTENTS

FIGURES

I. INTRODUCTION

Crises[1] are commonly seen in deterministic, dissipative, nonlinear dynamical systems, and they have been demonstrated in many experimental[2,3] and numerical studies. In a crisis, one of several characteristic changes in a chaotic attractor takes place as a system parameter p passes through some critical value p_c, at which the crisis occurs: the chaotic attractor may be destroyed, it may increase in size, or it may merge with some other chaotic attractor. As detailed in the next paragraph, typical trajectories of a post-critical system (by convention $p > p_c$) behave like those of the pre-critical system for a time that is sensitively dependent on initial conditions. For $p>p_c$ and randomly chosen initial conditions in the basin of the pre-critical $p<p_c$ attractor, the length of this time T is found to be exponentially distributed,[4] with a mean length τ that depends on p; *i.e.*, the probability density of T is $P_T(t)=\tau^{-1}e^{-t/\tau}$, $t>0$.

The definition of the characteristic time τ differs for the three types of crises mentioned above. In the case of attractor destruction, the trajectory initially moves chaotically as though it were still confined to the pre-critical attractor, and then leaves the region in phase space where the former attractor was located, and tends to some other attractor, or possibly to infinity. The period of time that the post-critical system behaves like the pre-critical system is referred to as a chaotic transient. For this case τ is the length of the transient, averaged over many different initial conditions. In the case of attractor enlargement, the post-critical trajectory stays in the phase space region of the the pre-critical chaotic attractor for some time, and then bursts into chaotic motion over a larger region in phase space, before being reinjected into the region of the pre-critical attractor; the process then repeats. For this case, τ is the average time between such bursts. In the case of attractor merging, which can occur in systems with symmetries, the post-critical motion switches repeatedly between the phase-space regions occupied by the pre-critical

chaotic attractors that merge at the crisis. The characteristic time τ is now the average time between switchings.

For a large class of low-dimensional systems (including one-dimensional maps, and many two-dimensional maps and three-dimensional flows), the characteristic time τ is found to scale with the parameter as[5]

$$\tau \sim |p - p_c|^{-\gamma}. \tag{1}$$

The crises with such scaling behavior result from the collision of the chaotic attractor with the stable manifold of an unstable periodic orbit. In particular, when we consider two-dimensional maps or three-dimensional flows, we are interested in cases where the collision is a tangency between the stable manifold of an unstable periodic orbit and the unstable manifold of the same (homoclinic tangency crisis) or another (heteroclinic tangency crisis) unstable periodic orbit. The critical exponent γ in the scaling law (1) is determined by the eigenvalues of the periodic orbit whose unstable manifold is involved in the tangency[5] (or is $\frac{1}{2}$ for one-dimensional maps with generic, quadratic maxima).

In a deterministic system for $p<p_c$, the characteristic time is infinite, because the orbit remains forever on the pre-critical attractor. However, if some random noise is added to the system, there is the possibility that a trajectory starting in the basin of attraction of the deterministic system's chaotic attractor will behave like an orbit of the post-critical system even for $p<p_c$, thereby producing a transient response. For example, in the cases of attractor destruction and merging, noise can kick an orbit across the boundary of the attractor's basin of attraction. This situation is referred to as a *noise-induced crisis*, and it stands in contrast to those metastable situations where the corresponding deterministic system is neither chaotic nor near crisis. Because real physical systems are always accompanied by noise, we believe that noise-induced crises may be an important complication in the experimental investigation of transient chaos. Alternatively, the intentional addition of noise to an experiment may offer another

dimension of control in understanding the underlying crisis dynamics. It is the purpose of this dissertation to provide a theory, supported by numerical and physical experiments, for the effects of noise on crises.

The production of metastable states in dynamical systems by the introduction of noise has been considered in the literature of physics and stochastic processes for many years.[6] The usual approach has been to describe the evolution of a probability density by a partial differential equation, obtaining state lifetimes by determining the rate at which probability mass passes through some boundary in phase space. Such an approach is in principle applicable to noise-induced crises, but the underlying nonlinear dynamics typically make for an intractable density-evolution equation.

The effects of noise on transitions to chaos via the period-doubling and intermittency routes have been considered previously.[7] Numerical studies of noise-induced crises have also been performed.[8,9] In Ref. 9, which included numerical experiments and an analysis of a one-dimensional map, it was suggested that noise-induced crises may admit scaling behavior for their characteristic times. In this dissertation, we argue that for noise-induced crises, corresponding to deterministic crises with scaling behavior (1), the characteristic time scales as

$$\tau \sim \sigma^{-\gamma}\, g\left(\frac{p_c - p}{\sigma}\right), \tag{2}$$

where σ is a measure of the strength of the noise, $g(\bullet)$ is a non-universal function depending on the system and the distribution function of the noise, and γ is the critical exponent of the corresponding *deterministic* crisis. We obtain this result without recourse to density-evolution partial differential equations. [Note that consistency of (1) and (2) implies that $g(-x) \sim x^{-\gamma}$ for large positive x.]

In Chapter II, we derive scaling law (2), starting with one-dimensional maps and generalizing to higher dimensions. We also review the deterministic theory

leading to scaling law (1), because it determines the critical exponent in the new scaling law (2), and underlies certain features seen in the numerical examples with noise discussed later.

Chapter III presents a more detailed analysis of the one-dimensional map discussed in Ref. 9. In determining the function $g(\bullet)$ of Eq. (2) explicitly for this case (something we are unable to do for the more complicated examples), we emphasize how certain simplifying assumptions made in the derivation of Eq. (2) affect the accuracy and applicability of the scaling law. We then outline the procedures used to get the numerical results in the balance of this dissertation. Numerical results for the one-dimensional map show that Eq. (2) is satisfied for this case (see also Ref. 9), and support the exponential distribution of τ.

Chapter IV includes two examples of two-dimensional maps, which have deterministic crises with critical exponents depending on the eigenvalues of mediating unstable saddles. One, with a heteroclinic tangency crisis, is used to demonstrate the effect of the noise distribution function on the function $g(\bullet)$. The other system demonstrates that (2) works equally well for a homoclinic tangency crisis.

In Chapter V, we discuss two potential complications to observing scaling law (2). In the first example, we discuss circumstances that produce results clustering around, rather than on, the curve given by the function $g(\bullet)$. A second example shows how the presence of noise can lead to trajectories escaping via routes different from those of the corresponding deterministic crisis; such alternate routes of escape produce a more stringent bound on σ than would otherwise be required for scaling to be observed.

Although the derivation of scaling law (2) in Chapter II considers only maps, in Chapter VI we discuss its applicability to flows as well, and present a supporting numerical example in which the noise is introduced in a physically motivated way to produce a stochastic differential equation.

In Chapter VII, we discuss the implications of Eq. (2) for experiments studying transient chaos, and in Chapter VIII, we describe a physical experiment confirming for the first time the applicability of Eq. (1) [specifically, the prediction of γ in Eq. (1)] and Eq. (2) to physical systems. The final chapter briefly summarizes our conclusions. Three appendixes contain technical details of the derivation of $g(\bullet)$ for the logistic map, of the integration schemes used to study the stochastic differential equation, and of the estimation of eigenvalues of unstable periodic orbits from experimental time series.

II. DERIVATION OF SCALING LAW (2)

A. One-dimensional maps

As discussed in Chapter I, we are interested in crises which result from the collision of a chaotic attractor with the stable manifold of an unstable periodic orbit. For concreteness, consider a crisis in one dimension mediated by an unstable fixed point. The system is governed by the one-dimensional map

$$x_{n+1} = F(x_n; p) + Z_n, \tag{3}$$

where $F(\bullet)$ is the deterministic map, and the Z_n are independent, identically distributed random variables with density function $P_Z(z)$. The deterministic crisis occurs when, as the parameter is increased through p_c, the chaotic attractor (an interval) collides with the unstable fixed point. We treat only nondegenerate crises, that is those where the distance ε from the attractor to the mediating unstable fixed point scales linearly with $p_c - p$ for p near p_c. The noise-induced crisis results from noise kicking a trajectory across the ε-gap (or its preimage) between the attractor and the mediating unstable fixed point (or its preimage).

We estimate the rate at which such events occur, using several simplifying assumptions to apply random variable techniques. The procedure is illustrated schematically in Fig. 1. First, we suppose that the invariant density for the deterministic attractor at $p = p_c$ does not change in form as p is decreased slightly, but rather that the attractor measure simply shifts away from the fixed point linearly with $p_c - p$. In Fig. 1(a) the attractor measure is schematically represented as a smooth function which is zero within a distance $\varepsilon \sim p_c - p$ from the fixed point. We further assume that iterates of the map can be treated as independent realizations of a random variable with density function equal to the invariant density of the deterministic attractor. Obviously, this assumption ignores the dynamics near the fixed point. However, the analysis of the logistic map

given in the next section will show how consideration of the detailed dynamics in the immediate vicinity of the fixed point leaves the form of the scaling law unchanged. We therefore only require sequences of iterates in the vicinity of the fixed point ("close approaches") to be sufficiently separated in time and sufficiently uncorrelated to provide a Poisson process for the close approaches. But this is only the same requirement as for scaling law (1) to apply, and is satisfied by the chaotic dynamics.

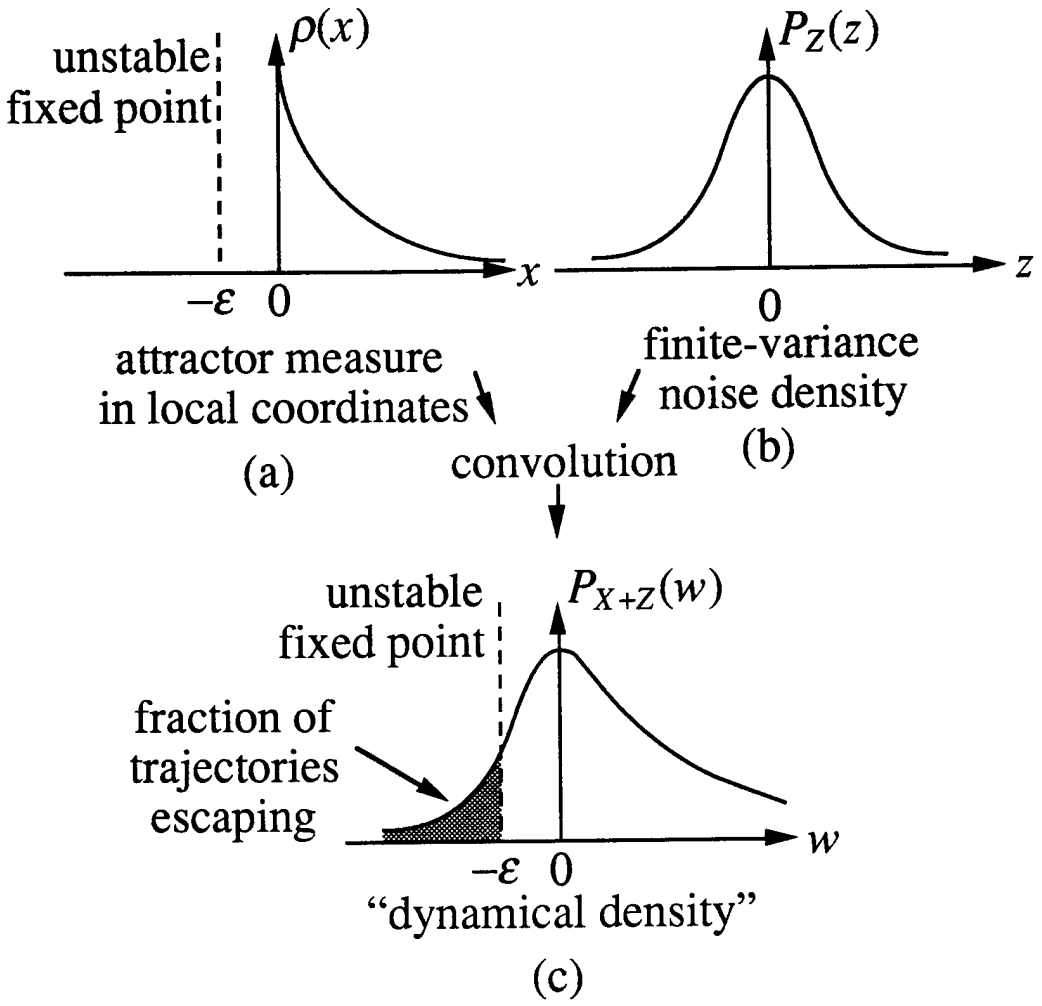

FIG. 1. The natural measure of the attractor, here drawn as smooth, is treated like the density of a random variable and convolved with the noise density to produce the dynamical density from which the escape rate is calculated.

We account for the addition of noise to the system by convolving the invariant density of the attractor with the density function of the noise [Fig. 1(b)] to construct a "dynamical density" [Fig. 1(c)]. Note the implicit assumption that the additive noises ..., $Z_{n-3}, Z_{n-2}, Z_{n-1}$ have no effect on the density of x_n. We associate the probability mass falling on the other side of the unstable fixed point from the deterministic attractor with those trajectories that terminate the transient response of the metastable system. Thus we calculate the characteristic time for the noise-induced crisis as proportional to the reciprocal of the escaping probability mass. This ignores orbits that escape from the attractor and are then reinjected by the noise (as well as all higher-order contributions), but as we will show in Chapter III, the linear scaling of the close approach region on forward or backward iteration of the map means that all such contributions will scale the same way, and hence do not alter the form of Eq. (2).

We make two further assumptions to derive scaling form (2) via dimensional analysis. First, we assume that the invariant density of the attractor, expressed in the local coordinates of Fig. 1 and for small, positive x can be written as $\rho(x) \sim x^{\gamma-1}$ [for $x<0$, $\rho(x)=0$)] For one-dimensional maps, the critical points [*i.e.*, the maxima and minima of $F(\bullet)$] are generically quadratic. This leads to γ being generically $\frac{1}{2}$ for one-dimensional maps. For non-generic cases when x is near a critical point x_c, we have $F(x) \approx F(x_c)+K|x-x_c|^{\delta}$, ($\delta \neq 2$), and the exponent γ is[10] $1/\delta$. We therefore leave γ general. Second, we assume that the density of the additive noise $P_Z(z)$ falls off rapidly enough with z that various limit and asymptotic substitutions in the following derivation introduce negligible error. The reciprocal of the characteristic time τ is proportional to the shaded probability mass in Fig. 1(c), which is the definite integral of a convolution:

$$1/\tau \sim \int_{-\infty}^{-\varepsilon} dw\, P_{X+Z}(w) = \int_{-\infty}^{-\varepsilon} dw \int_{-\infty}^{\infty} dx\, \rho(x)\, P_Z(w-x).$$

Substituting the asymptotic form of $\rho(x)$ and writing $P_Z(z)$ in the natural form $\sigma^{-1}\, q(z/\sigma)$, where σ is the scale length of the noise, we have:

$$1/\tau \sim \int_{-\infty}^{-\varepsilon} dw \int_{-\infty}^{\infty} dx \frac{1}{\sigma} q\left(\frac{w-x}{\sigma}\right) \Theta(x) x^{\gamma-1},$$

(where $\Theta(\bullet)$ denotes the unit step function). Making the change of variables $y=x/\sigma$, and doing the second integral by parts (the surface terms vanish because the noise density vanishes at infinity and the invariant density in Fig. 1(a) vanishes for $x<0$), we have:

$$1/\tau \sim \sigma^{\gamma-1} \int_{-\infty}^{-\varepsilon} dw \int_{0}^{\infty} dy\, q'(w/\sigma - y)\, y^{\gamma}.$$

Naming the second integral (a function only of w/σ) $r(\bullet)$ and making the final substitution $s=w/\sigma$ yields:

$$1/\tau \sim \sigma^{\gamma} \int_{-\infty}^{-\varepsilon/\sigma} ds\, r(s).$$

Naming the remaining integral (a function only of ε/σ) $1/g(\bullet)$, we obtain scaling form (2). Thus the critical exponent of the deterministic system, fixed by the properties of the measure of the near-critical attractor, also governs the transient response of the noisy system.

B. Two-dimensional maps

Noisy two-dimensional maps of the form

$$\mathbf{x}_{n+1} = \mathbf{F}(\mathbf{x}_n; p) + \mathbf{Z}_n, \tag{3'}$$

where now $\mathbf{x}$, $\mathbf{F}$, and $\mathbf{Z}$ are vector-valued, can also be considered. This situation is more complicated, because at crisis the unstable manifold of the mediating fixed point has an infinite number of tangencies with the stable manifold with which it collides. Furthermore, these tangencies may have different orientations in phase space, and the noise density $P_{\mathbf{Z}}(\mathbf{z})$ may be anisotropic. However, the various tangencies are again locally only linear rescalings of one another. By projecting both the attractor's invariant measure and the noise density onto an axis normal to the stable manifold in the vicinity of each tangency (as illustrated in Fig. 2), the analysis for one-dimensional systems can be applied as before, where the local, one-dimensional coordinate of the stable manifold takes the place of the unstable fixed point in the one-dimensional case. Noise anisotropy may change the contributions of the various tangencies to the total escape rate, relative to isotropic noise, but should not typically change scaling form (2), where now γ is fixed by the properties of the measure of the higher-dimensional chaotic attractor.

A difference from the one-dimensional situation is that the critical exponent γ is no longer generically confined to be $\frac{1}{2}$. Reference 5 derived formulas for determining the critical exponent governing a deterministic crisis in a two-dimensional map. These derivations are reviewed here, because they help to explain several aspects of the numerical examples to be discussed in later sections.

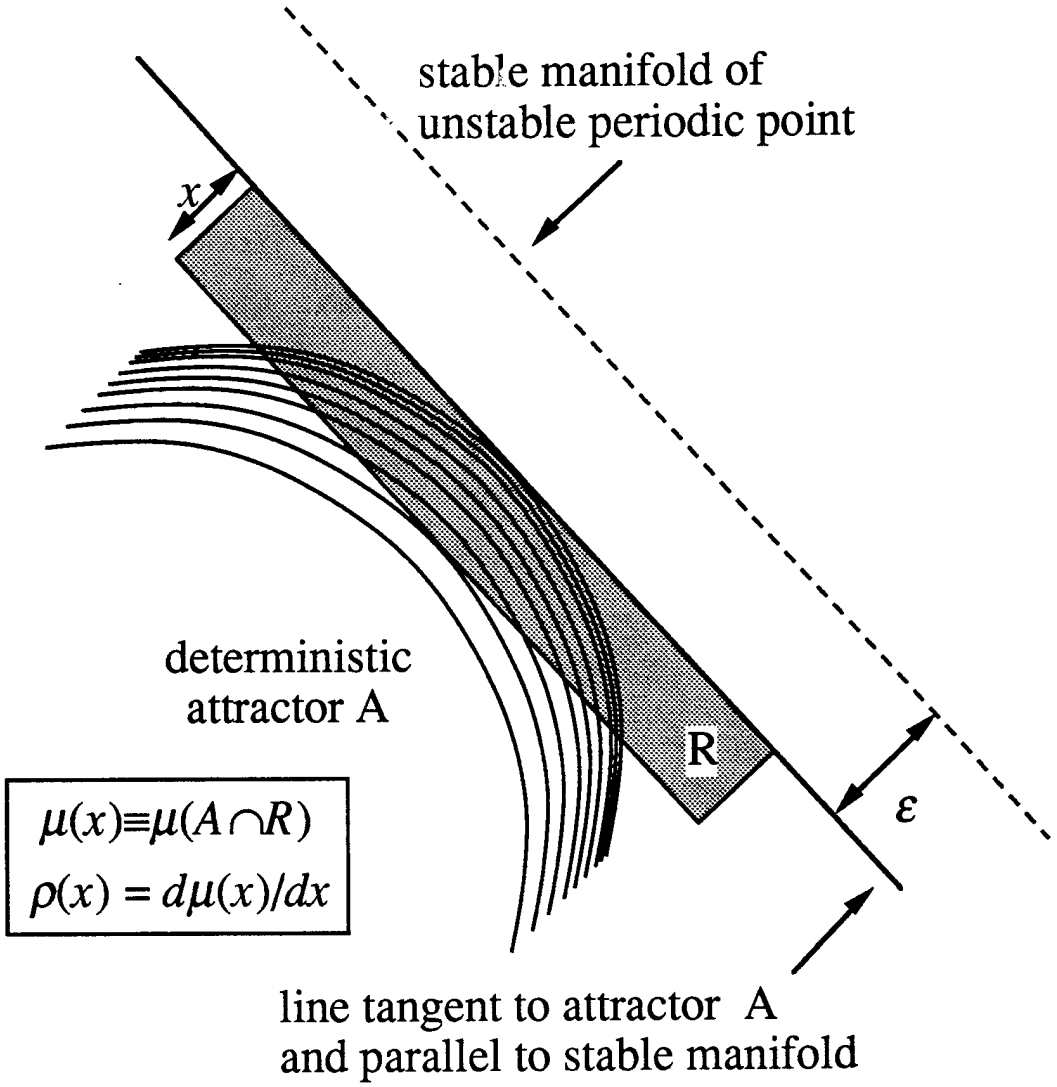

FIG. 2. For two dimensional maps, the natural measure of the attractor is projected into one dimension running normal to the mediating stable manifold, before being convolved with the similarly-projected noise density. Region R is a rectangular strip of width x, with only those parts of its boundary that are parallel to the stable manifold intersecting the attractor.

The tangency causing the crisis can occur in two possible ways.

(i) Heteroclinic tangency. In this case, the stable manifold of an unstable periodic orbit (B) is tangent to the unstable manifold of an unstable periodic orbit (A) on the attractor, as in Fig. 3(a). (Figure 3 is drawn for the case of fixed points; for the case where A and B are periodic points, similar pictures can be drawn.)

(ii) Homoclinic tangency. In this case, the stable and unstable manifolds of an unstable periodic orbit (B) are tangent, as in Fig. 3(b).

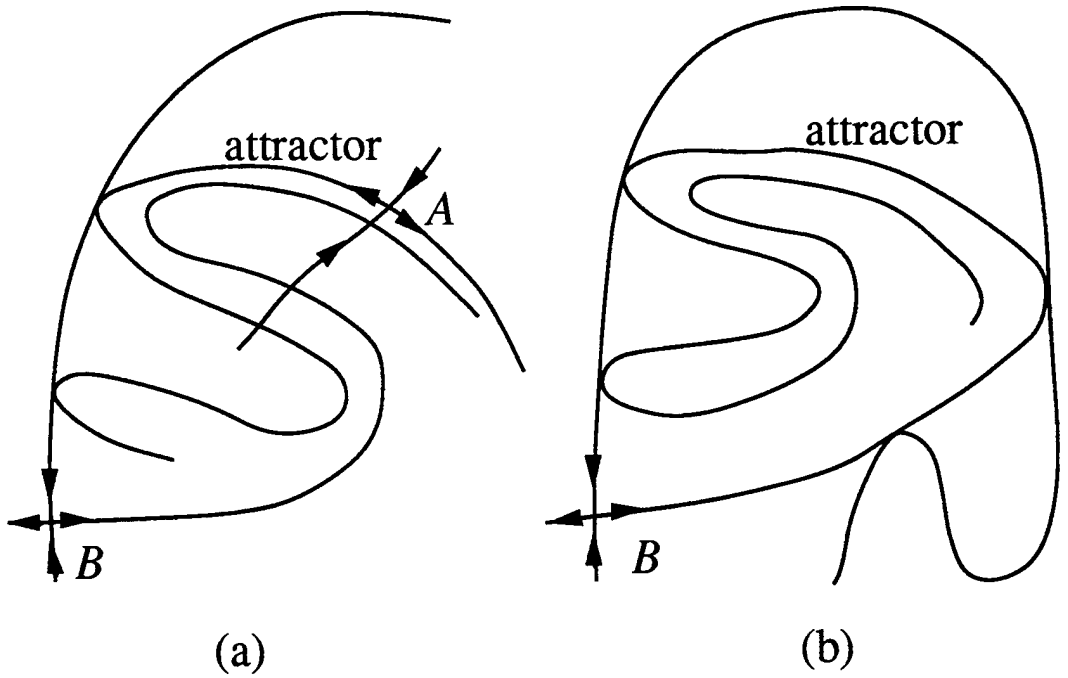

FIG. 3. (a) Schematic illustration of heteroclinic tangencies of the stable manifold of the unstable periodic orbit B and the unstable manifold of the unstable periodic orbit A. (b) Schematic illustration of homoclinic tangencies of the stable and unstable manifolds of the unstable periodic orbit B. The figure is drawn for period-1 orbits.

As in the one-dimensional case, we assume that the crisis is nondegenerate, and further that the tangency is quadratic. In both cases, at $p=p_c$ the chaotic attractor is the closure of one of the branches of the unstable manifold of B. In the heteroclinic case, the critical exponent is given by

$$\gamma = \frac{1}{2} + ln|\alpha_1| \, (|ln|\alpha_2||)^{-1}, \tag{4}$$

where α_1 and α_2 are the expanding ($|\alpha_1|>1$) and contracting ($|\alpha_2|<1$) eigenvalues, respectively, of the periodic orbit A in Fig. 3(a). In the case of a homoclinic tangency, we have

$$\gamma = ln|\beta_2| \, / \, ln|\beta_1\beta_2|^2, \tag{5}$$

where β_1 and β_2 are the expanding and contracting eigenvalues of the periodic orbit B in Fig. 3(b). For both cases, letting the contraction rate be large ($|\alpha_2|^{-1}, |\beta_2|^{-1} \rightarrow \infty$) recovers the generic exponent for one-dimensional maps, $\gamma=\frac{1}{2}$.

For the heteroclinic crisis, as p is increased past p_c, the unstable manifold of A crosses the stable manifold of B (cf. Fig. 4). Before the crisis the attractor was confined to the region to the right of the upper stable manifold segment of B, and B is not on the attractor After the crisis an orbit initially in the region in which the chaotic attractor was confined for $p<p_c$ can eventually land in the shaded region ab of Fig. 4. Such an orbit will then be attracted along the stable manifold of B and then rapidly leave the region to which the chaotic attractor was confined along the left branch of the unstable manifold of B. For p near p_c, the dimensions of region ab are of order r and $r^{1/2}$, where $r \sim p-p_c$. We now iterate the region ab backwards in time for n steps. For small r and large enough (but not too large) n, except for the first few backward iterates, the change in the region ab is governed by the linearization of the map about A. Thus the preiterated region $a'b'$ has dimensions of the order r/α_2^n and $r^{1/2}/\alpha_1^n$, as shown in Fig. 4.

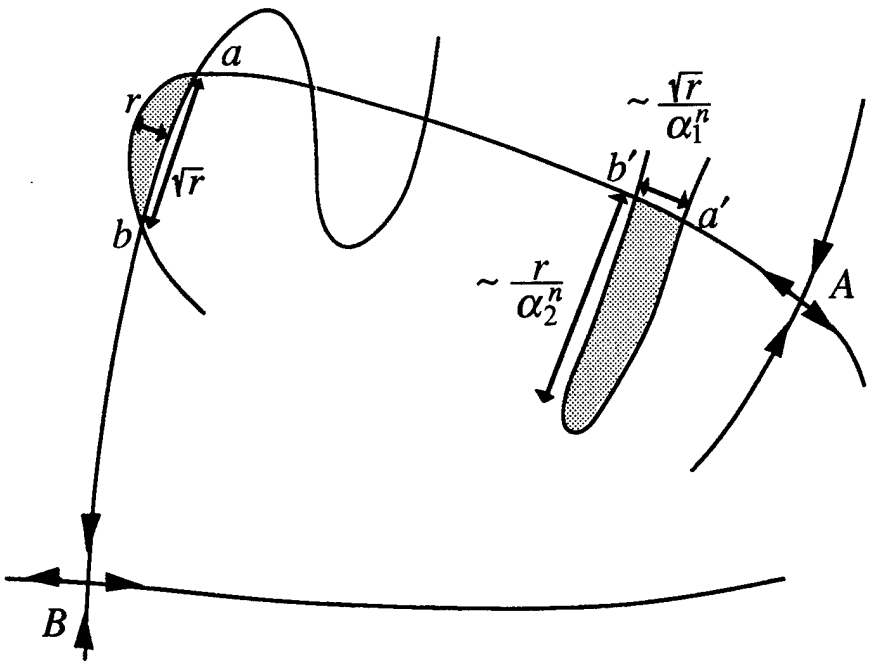

FIG. 4. Schematic diagram illustrating the derivation of Eq. (4)

Because after falling in region $a'b'$ the orbit soon falls in region ab, we estimate τ as the average time it takes an orbit to land in region $a'b'$. Now consider the probability measure of the attractor at $p=p_c$. The quantity τ^{-1} is then estimated as the probability that, on a given iterate, an orbit on the $p=p_c$ attractor falls in the region $a'b'$, and we denote this probability by $\mu(r)$. Now reduce r by the factor α_2 and consider the resulting region ab. After we iterate backwards $n+1$ steps (instead of n), the long dimension of the preiterated region is again r/α_2^n but the width is changed to $(\alpha_2 r)^{1/2}/\alpha_1^{n+1}$. Assuming that, for our purposes, the attractor measure can be treated as if it were smooth in the direction of the unstable manifold of A, we have

$$\frac{\mu(r)}{\mu(\alpha_2 r)} \sim \frac{r^{1/2}/\alpha_1^n}{(\alpha_2 r)^{1/2}/\alpha_1^{n+1}} = \frac{\alpha_1}{\alpha_2^{1/2}}.$$

With the assumption that $\mu(r) \sim r^{\gamma}$, Eq. (4) then follows. [Actually $\mu(r)$ is typically not smooth. For the purposes of this dissertation it suffices to treat it as if it is smooth.]

For the homoclinic case, consider the situation at $p=p_c$ represented schematically in Fig. 5. We denote the measure of the attractor in the shaded region defined by the unstable manifold segment *aoc* and the vertical line *abc* by $\mu(\varepsilon)$, where we take the vertical line *abc* to be distance ε from the stable manifold of B. We assume that $\mu(\varepsilon)\sim\varepsilon^{\gamma}$, for small ε, and, as above, identify the exponent for $\mu(\varepsilon)$ with that governing the scaling of the characteristic time. The basis for this assumption is that for p slightly greater than p_c, we expect the unstable manifold of B shown to poke over to the other side of the stable manifold by a distance $\varepsilon \sim p-p_c$, as in Fig. 4. Thus we have $\tau^{-1}\sim\mu(\varepsilon)$

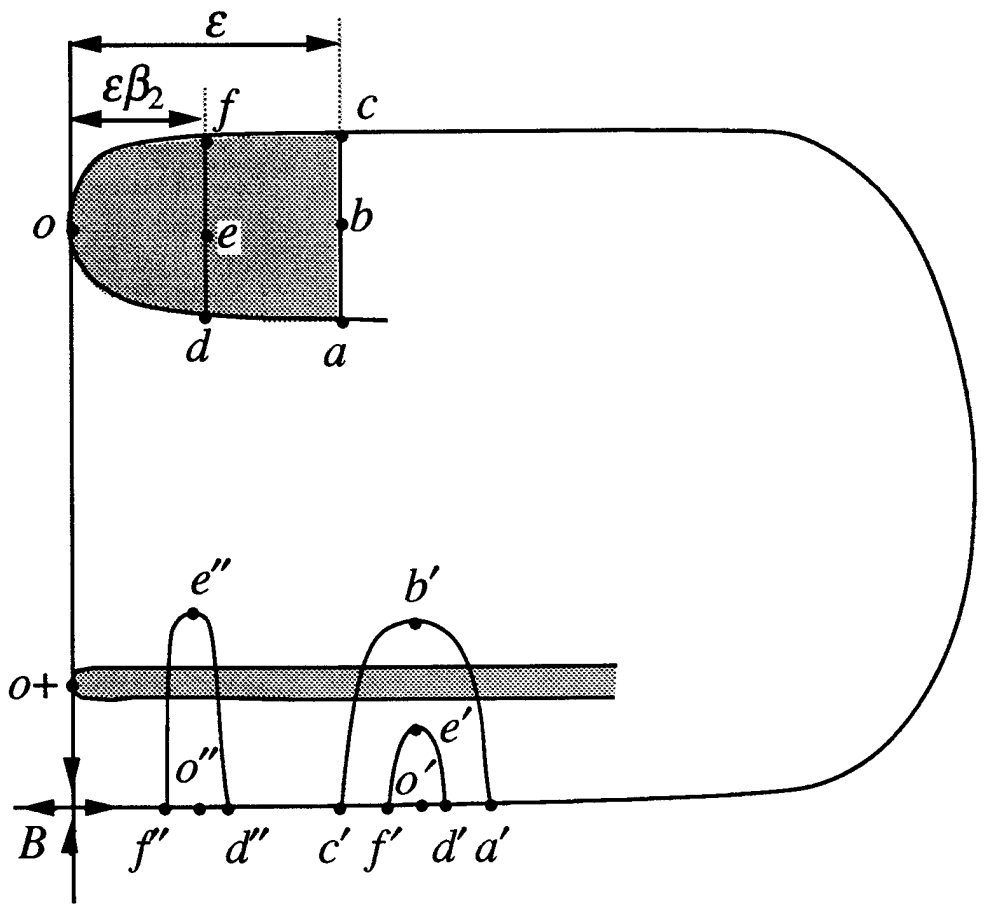

FIG 5. Schematic diagram illustrating the derivation of Eq. (5)

Also shown in Fig. 5 is another vertical line segment *def* which has been chosen a distance $\varepsilon\beta_2$ from the stable manifold of B. The measure of the attractor in the region *defod* is $\mu(\varepsilon\beta_2)$. Our goal in what follows will be to estimate the ratio $\mu(\varepsilon\beta_2)/\mu(\varepsilon)$. By doing this we shall be able to determine the exponent γ.

Imagine that we iterate the shaded region backward in time many iterates so that the points (a, b, c, d, e, f, o) map to $(a', b', c', d', e', f', o')$ which are close to B (for ε small). Now iterate the region $d'e'f'o'd'$ backward one further iterate to $d''e''f''o''d''$. Because the primed letters are close to B this one further backward iterate is governed by the linearized map at B (*i.e.*, by the eigenvalues β_1 and β_2 evaluated at B). Thus the distance from o' to e' is stretched by β_2^{-1} to $o''e''$, while segment $f'o'd'$ is compressed by β_1^{-1} to become the shorter segment $f''o''d''$. Note, however, that because the original distance from o to e (namely, $\varepsilon\beta_2$) was chosen to be shorter by precisely the factor β_2 than the distance from o to b (namely, ε), we now have that the distance from e'' to o'' is the same as that from b' to o'. Also, because the tangency of the stable and unstable manifolds at o is quadratic, we have that the curve segment *fod* is shorter than the curve segment *coa* by $\sqrt{\beta_2}$. Because ε is small, this also implies that the segment $f'o'd'$ is shorter than $c'o'a'$ by $\sqrt{\beta_2}$. By putting these facts together we summarize the relevant information as follows:

$$\overline{(o'b')} = \overline{(o''e'')}, \tag{6}$$

$$\overline{(c'o'a')} = \overline{(f''o''d'')}(\beta_1/\sqrt{\beta_2}), \tag{7}$$

where the superscripted bar denotes the length of the segment.

We now wish to obtain an estimate of the ratio of the measure of the attractor contained in the region $d''e''f''o''d''$ to the measure of the attractor contained in the region $a'o'c'b'a'$. To do this, imagine iterating the shaded region at the tangency o forward many iterates in time so that o maps to the point $o+$ in Fig. 5. The shaded region has now been greatly stretched out along the direction of the unstable manifold of B.

Because $d\mu(\varepsilon)/d\varepsilon \sim \varepsilon^{\gamma-1}$, we conclude that the amount of attractor measure per unit horizontal length contained in the shaded region emanating from $o+$ is larger in $d''e''f''o''d''$ than in $a'o'c'b'a'$ by the factor $\beta_1^{1-\gamma}$. The same result applies for other iterates of the shaded region. Thus using Eq. (7) we obtain

$$\frac{\mu(d''e''f''o''d'')}{\mu(a'o'c'b'a')} = \frac{\beta_2^{1/2}}{\beta 1}\beta_1^{1-\gamma}, \tag{8}$$

where $\mu(d''e''f''o''d'')$ represents the measure in $d''e''f''o''d''$ while $\mu(a'o'c'b'a')$ represents the measure in $a'o'c'b'a'$.

Because the region $d''e''f''o''d''$ maps to *defod*, the measure of the attractor inside $d''e''f''o''d''$ is just $\mu(\varepsilon\beta_2)$. Similarly, the measure of the attractor inside $a'o'c'b'a'$ is $\mu(\varepsilon)$. Thus, because $\mu(\varepsilon)\sim\varepsilon^{\gamma}$, we also have

$$\frac{\mu(d''e''f''o''d'')}{\mu(a'o'c'b'a')} = \beta_2^{\gamma}. \tag{9}$$

By combining Eqs. (8) and (9) we have

$$\beta_2^{1/2} = (\beta_1\beta_2)^{\gamma},$$

which yields the desired result, Eq. (5) for γ.

Finally, although we have not done numerical experiments with noisy D-dimensional maps (D>2), we conjecture that scaling form (2) will apply to many situations in higher dimensions also, if Eq. (1) applied in the absence of noise. The projection procedure used to reduce the two-dimensional case to the one-dimensional case could also be applied to higher dimensional systems. The main requirement for scaling form (2) to apply to a higher dimensional situation is that the measure of the attractor accumulate as $\mu(\varepsilon)\sim\varepsilon^{\gamma}$ near the edge of the attractor. Reference 5 (1987) discussed the generalization of Eq. (4) to smooth D-dimensional maps, for the case where there is an attractor containing an unstable periodic orbit with D–1 unstable eigenvalues

and one stable eigenvalue, and the attractor undergoes the D-dimensional analog of a heteroclinic tangency crisis. This particular generalization conformed to the required scaling for the measure. Physical experiments have been done producing chaotic attractors in the Poincaré section having correlation dimensions greater than 2 which also demonstrated the required scaling for the measure.[3] However, in those, and indeed most, higher dimensional cases there is as yet no theoretical basis for predicting the critical exponent γ. This is one reason why noise may be useful as an experimental probe in physical systems, where scaling form (2) may complement scaling form (1) in investigating critical phenomena.

III. THE NOISY LOGISTIC MAP

In this section, we estimate analytically the characteristic time τ of a particular, one-dimensional noise-induced crisis resulting in attractor destruction. This case was first discussed in Ref. 9. We show that the dynamics of successive iterates of the system near the crisis-mediating fixed point, which contribute to high order effects such as orbits leaving and reentering the basin of attraction, do not affect the validity of scaling form (2). We also discuss numerical experiments performed on the system, which demonstrate that: (i) the transient length T is exponentially distributed, as implied by the derivation of scaling form (2), and (ii) our analytical estimate of τ, which conforms to scaling law (2), agrees with the numerical results over a range of parameters, suggesting that the asymptotic scaling form (2) is in fact observable in practice.

The noisy logistic map is given by

$$x_{n+1} = p\, x_n\,(1 - x_n) + Z_n. \tag{10}$$

We consider the case where the Z_n are independent, identically distributed Gaussian random variables with variance σ^2. [In this dissertation, we will denote a Gaussian probability density with mean m and variance σ^2 as $N(\bullet;m,\sigma^2)$; a uniform probability density on an interval (a,b) will be denoted $U(\bullet;a,b)$.] It is well known that the deterministic (Z_n identically 0) analog of Eq. (10) at has a crisis at $p=p_c=4$ resulting in the destruction of a chaotic attractor covering the interval [0,1]. Further, at $p=4$ the chaotic attractor has invariant measure given by[11]

$$\rho(x) = \frac{1}{\pi\sqrt{x(1-x)}}.$$

For p slightly less than 4, the attractor is reduced in size to the interval $[4-p,p/4]$. For our purposes, in what follows we assume that the measure for p slightly less than 4 can be approximated by

$$\rho(x) \approx \frac{1}{\pi\sqrt{p/4-x}}\,\Theta(p/4-x)\,,$$

for x near $p/4$; for σ small enough, we do not care about the form of $\rho(x)$ outside this neighborhood. The dynamical density $P_{X+Z}(w)$ can be obtained by convolving $P_Z(z)$ and $\rho(x)$. This density has a nonzero tail to the right of w=1, *i.e.* outside the attractor's basin of attraction. We estimate a contribution R (escapes to the right) to the overall escape rate by integrating $p_{X+Z}(w)$ over [1,∞), obtaining

$$R = \sigma^{1/2}\frac{1}{\pi\sqrt{2}}exp\left[-\left(\frac{p_c-p}{\sigma}\right)^2\frac{1}{64}\right]D_{-3/2}\left(\frac{1}{4}\frac{p_c-p}{\sigma}\right), \qquad (11)$$

where $D_k(x)$ is the parabolic cylinder function.[12] Equation (11) was obtained in Ref. 9, and was used to suggest that scaling laws similar to those applicable in noisy period-doubling cascades and intermittency[7] should also apply to noise-induced crises. Because the critical exponent γ for this one-dimensional crisis is $\frac{1}{2}$, and taking $\tau \sim R^{-1}$, Eq. (11) conforms to scaling law (2).

By applying the map (10) to the dynamical density, it is possible to obtain analytical estimates for the fraction $\overline{R}$ of the escapes contributing to R that fail because the noise reinjects the orbit into the basin of attraction on the next iterate, and also for the rate L of escape from the left side of the attracting interval. The derivation is outlined in Fig. 6. and done in detail in Appendix A. The right-hand escape rate R was obtained by integrating the dynamical density $P_{X+Z}(w)$ over [1,∞) [cf. Fig. 6(a)]. By applying the deterministic part of the map (10) to the density $P_{X+Z}(w)$, one obtains the density of orbits before they are kicked by noise on the next iterate, $\tilde{P}_{X+Z}(w)$ [cf. Fig. 6(b)]. Convolving the noise density with that part of $\tilde{P}_{X+Z}(w)$ to the right of w=0, and integrating the convolution over (–∞,0], one obtains an estimate of the left-hand escape rate L [cf. Fig. 6(c)]. This approach assumes that most of the left-hand escapes will in fact be not-quite-successful right-hand escapes. Because of the expansion produced by the unstable fixed point at 0, it becomes progressively less likely for an orbit to be kicked out of the left side of the attractor on successive iterates. Thus the assumption seems warranted. Alternatively, convolving the noise density with that part of $\tilde{P}_{X+Z}(w)$ to the

left of w=0, and integrating the convolution over (0,∞] yields an estimate of the rate $\overline{R}$ at which right-hand escaping orbits are kicked by the noise back into the basin of attraction (cf. Fig. 6(d)).

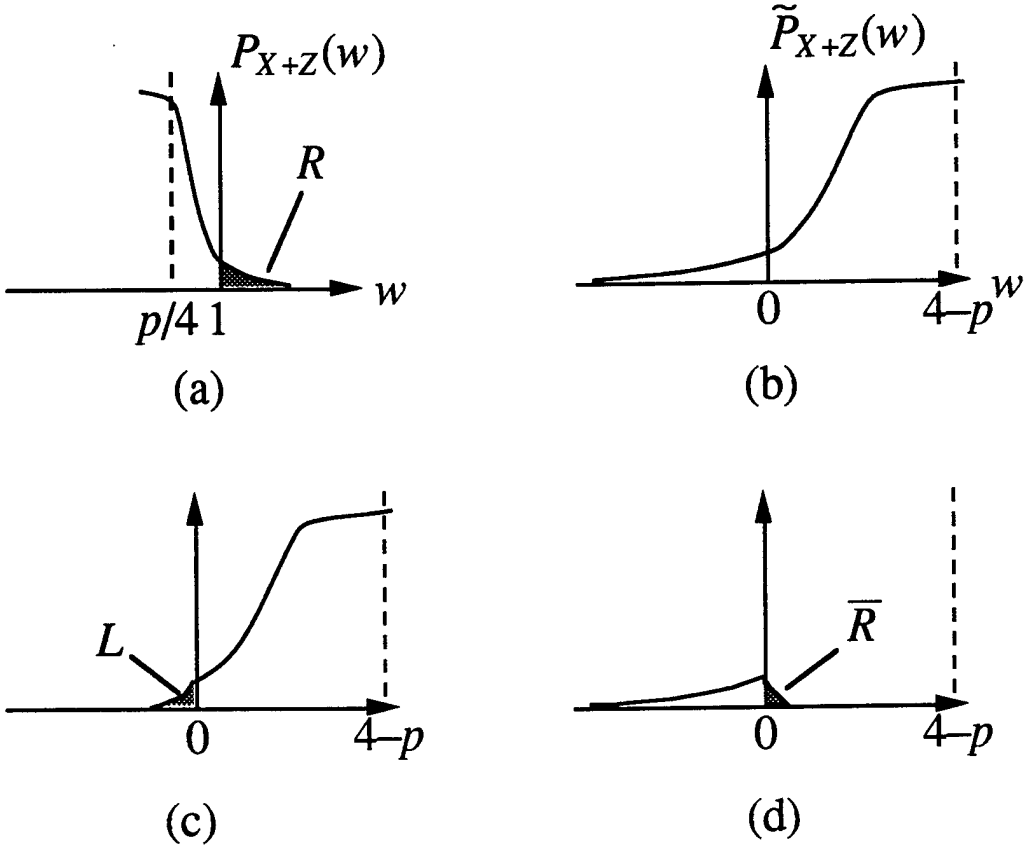

FIG. 6. (a) The right-hand escape rate for the noisy logistic map is obtained by integrating the dynamical density $P_{X+Z}(w)$ over [1,∞). (b) Applying the deterministic part of map (1) yields the density $\tilde{P}_{X+Z}(w)$ of orbits before the next noise kick. (c) and (d) The mapped density selectively convolved with the noise density allows estimation of the left-hand escape rate L and the right-hand failed-escape rate $\overline{R}$.

These higher-order contributions to the overall escape rate can be expressed as asymptotic expansions (see Appendix A):

$$\left.\begin{matrix} L \\ \overline{R} \end{matrix}\right\} \approx \frac{\sigma^{1/2}}{8\pi^{3/2}} exp\left[-\left(\frac{p_c - p}{\sigma}\right)^2 \frac{1}{64}\right] \times \sum_{k=0}^{k_{max}} \frac{\Gamma(k/2+1)(\pm 1)^k}{(k+1)!\, 2^{3k/2}} D_{k-1/2}\left(\frac{1}{4}\frac{p_c - p}{\sigma}\right) \quad \begin{matrix} (12) \\ (13) \end{matrix}$$

Therefore, an estimate of the characteristic time τ can be written as

$$\tau \approx [R - \overline{R} + L]^{-1}, \tag{14}$$

where one can see from Eqs. (11)–(13) that scaling form (2) with $\gamma = \frac{1}{2}$ applies. In addition to the three terms R, $\overline{R}$, and L, there will also be corrections due to higher order effects such as multiple crossings of the fixed point on successive iterations of the noisy map.

The derivation of the correction terms $\overline{R}$ and L shows that for a noise density $P_Z(z)$ that vanishes fast enough with z, the dynamics around the fixed point, which only linearly distort the overall picture from iterate to iterate, do not affect the final scaling form because we only assume a linear relation between $p_c - p$ and the distance from the attractor to the mediating fixed point; different constants of proportionality at each iterate generate contributions to τ that all scale like Eq. (2). Thus the higher-order terms do not change the scaling form (2).

Note also that although $\overline{R}$ is usually small compared to the other terms in Eq. (14), L tends to dominate R as $(p_c - p)/\sigma$ increases [$R \approx L$ when $(p_c - p)/\sigma = 12$]. This result differs from a conclusion of Ref. 9, where an estimate of L based on numerical experiments was given that underestimated its relative importance for large $(p_c - p)/\sigma$. Thus, the noise "causes" the crisis in different parts of the phase space, depending on its strength. This property could be important in the investigation of higher dimensional

physical systems, where the boundaries of basins of attraction can be much more complicated.

Numerical experiments were also performed with the noisy logistic map in the following way. Initial conditions were chosen at random in the deterministic attractor's basin of attraction, and were preiterated using the deterministic map at a specified parameter value, to obtain the natural measure of the attractor. Then the noisy map was applied, using a specified noise variance, until the orbit escaped from the basin of attraction. This was determined by waiting for the orbit to reach the region $x<-1$, where, for the values of σ used, the chances of the noise reinjecting the orbit into the interval [0,1] were negligible. Various diagnostics allowed determination of the relative contributions of the various terms in Eq. (14). An ensemble of transients was sampled for each set of parameters, allowing statistical estimation of the characteristic time τ. This general procedure was used for all of the numerical results presented in this dissertation, with specific criteria for deciding the end of a transient response depending on the particular system. Use of several different end criteria in a given system only changed the constant of proportionality in scaling laws. For all of the numerical experiments, pseudorandom numbers satisfied distribution and independence requirements to high statistical confidence levels.

Figure 7 shows a typical empirical distribution of transient lengths for the noisy logistic map. The cumulative distribution function $F_T(t)= \int_0^t P_T(s)ds$ for transient lengths T theoretically should be of the form

$$F_T(t) = 1 - exp(-t/\tau),\ t>0,$$

where τ is the characteristic time at the specified parameter value and noise strength. The sampled distribution is compared with this functional form, using the sample mean $<t>$ as an unbiased estimator of τ.

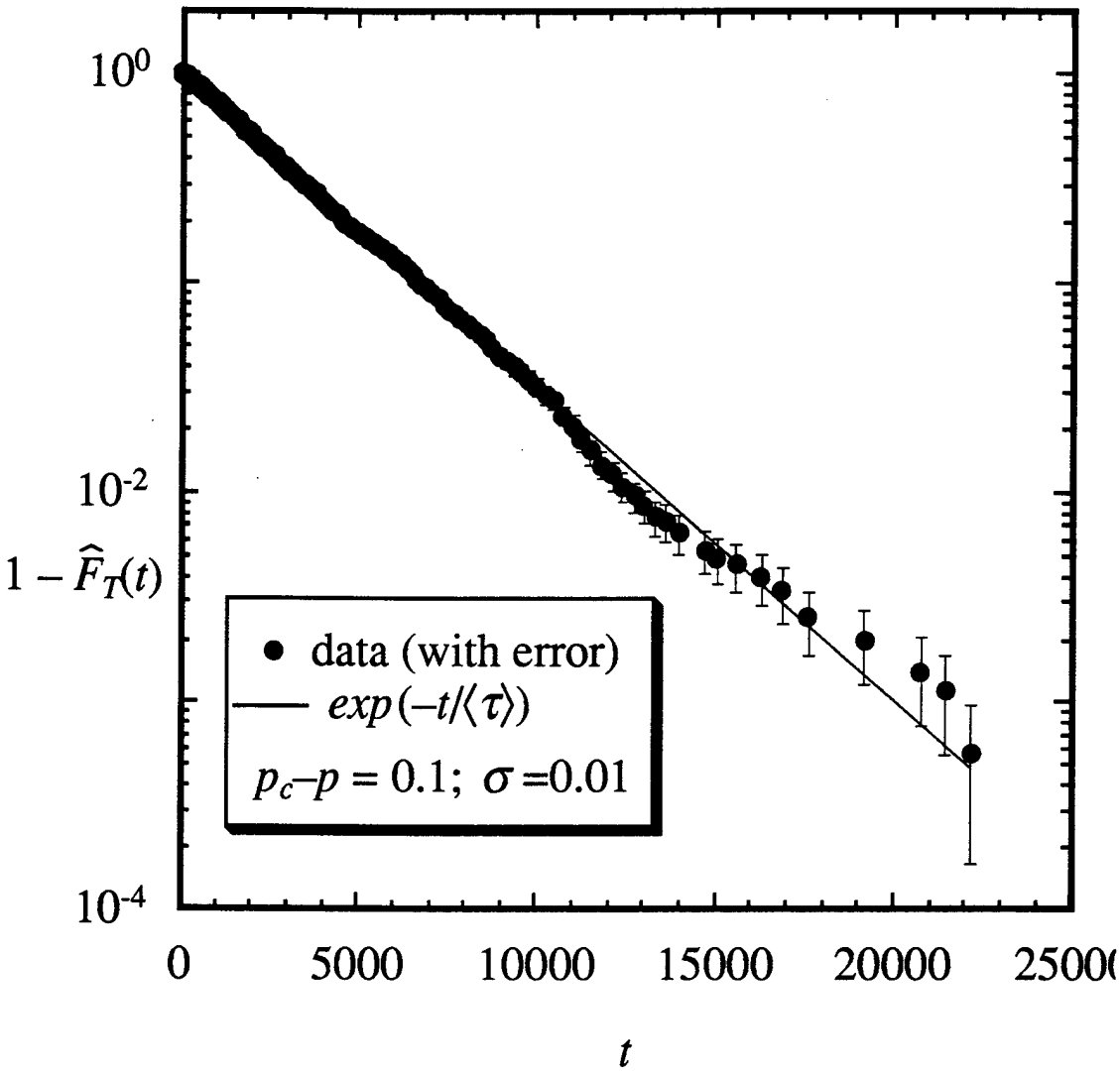

FIG. 7: The time (in iterations) taken by trajectories of the noisy logistic map to escape (specifically, to reach the region x<–1) from the deterministic basin of attraction is exponentially distributed. The straight line shows the theoretical form of the distribution, which is statistically consistent with the data. A Kolmogorov-Smirnov test indicated that the probability of the deviations from the theoretical distribution being as large as indicated due to chance is 0.38. In this and later figures, error bars indicate an approximately 68% probable (one standard deviation of the mean) confidence interval for the estimated quantity.

In Fig. 7 and what follows, we denote estimators of statistical quantities by a circumflex. The comparison is statistically significant, and combined with the results from 63 other ensembles at different parameter values, support the conclusion that the characteristic transient lengths T are exponentially distributed for noise-induced crises. This tends to vindicate the independence assumptions used in obtaining scaling law (2).

The numerical results are summarized in Fig. 8. Rewriting scaling law (2), we have

$$\tau \sigma^{\gamma} \sim g\left(\frac{p_c - p}{\sigma}\right), \tag{2'}$$

which implies that as $(p_c - p)/\sigma$ is varied, $\tau\sigma^{\gamma}$ should fall on a single curve [the graph of $g(\bullet)$] regardless of the value of σ. The results in Fig. 8 conform to this prediction for a range of σ spanning several orders of magnitude. Moreover, the numerical results agree with the analytically predicted form of $g(\bullet)$ based on Eqs. (11)–(14). Although not shown, the individual contributions R, $\overline{R}$, and L separately agree with the corresponding numerical results. For the results in Fig. 8, k_{max}=3 was used to evaluate Eqs. (11) and (12); $\overline{R}$ was about $0.1R$, and L ranged from about $0.1R$ at $(p_c - p)/\sigma$=0 to about $1.2R$ at $(p_c - p)/\sigma$=14.

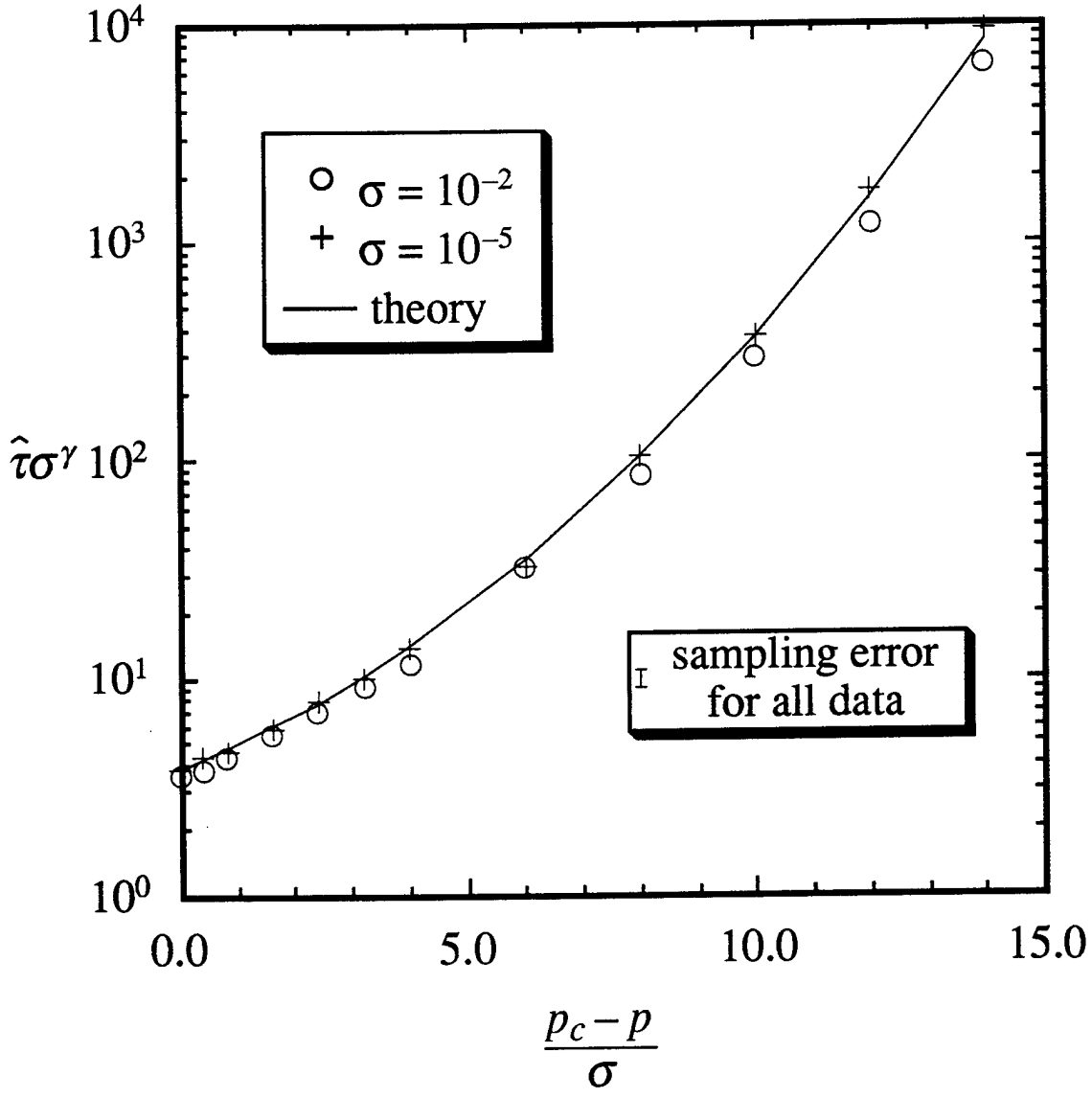

FIG. 8: The results of the numerical experiments with the noisy logistic map are statistically consistent with the theoretically-predicted scaling function given in Eqs. (11)–(14), for a three order-of-magnitude variation in the strength of the additive noise.

IV. NUMERICAL EXAMPLES USING NOISY TWO-DIMENSIONAL MAPS

In this section, we illustrate with numerical examples the application of scaling law (2) to two two-dimensional dissipative maps with noise, and demonstrate a restricted form of (2) reminiscent of scaling law (1), where the noise strength takes the role of the parameter excess $p-p_c>0$.

A. Hénon map; heteroclinic tangency crisis

The Hénon map was modified with additive noise to produce the system

$$\begin{aligned} x_{n+1} &= p - x_n^2 - Jy_n + Z_n^{(1)} \\ y_{n+1} &= x_n + Z_n^{(2)} \end{aligned} , \tag{15}$$

where the $\mathbf{Z}_n \equiv (Z_n^{(1)}, Z_n^{(2)})$ are independent, identically distributed two-vectors.

For $J=-0.3$, $p=p_c\approx 1.426\,921\,114$, the deterministic version of Eq. (15) has a heteroclinic tangency crisis, caused by an unstable fixed point [corresponding to B in Fig. 3(a)], which results in destruction of the chaotic attractor existing for $p\le p_c$. Based on the eigenvalues of an unstable fixed point on the attractor (corresponding to A in Fig. 3(a)), Eq. (4) yields a critical exponent for the deterministic scaling law (1) of $\gamma\approx 0.8557$. Previous numerical experiments with the deterministic system agreed with these theoretical results.[5] This value of γ was used to scale the data from numerical experiments on the noisy system of Eq. (15) for comparison with scaling law (2′), with the results shown in Fig. 9. For these experiments, the noise density used was $P_{\mathbf{Z}}(x,y)=N(x;0,\sigma^2)\delta(y)$. We are no longer able to provide a theoretical determination of the function $g(\bullet)$ (as was done in Chapter III) for comparison with the data, but the statistical consistency of the data over three orders of magnitude for the noise strength tends to confirm the applicability of Eq. (2) to this system.

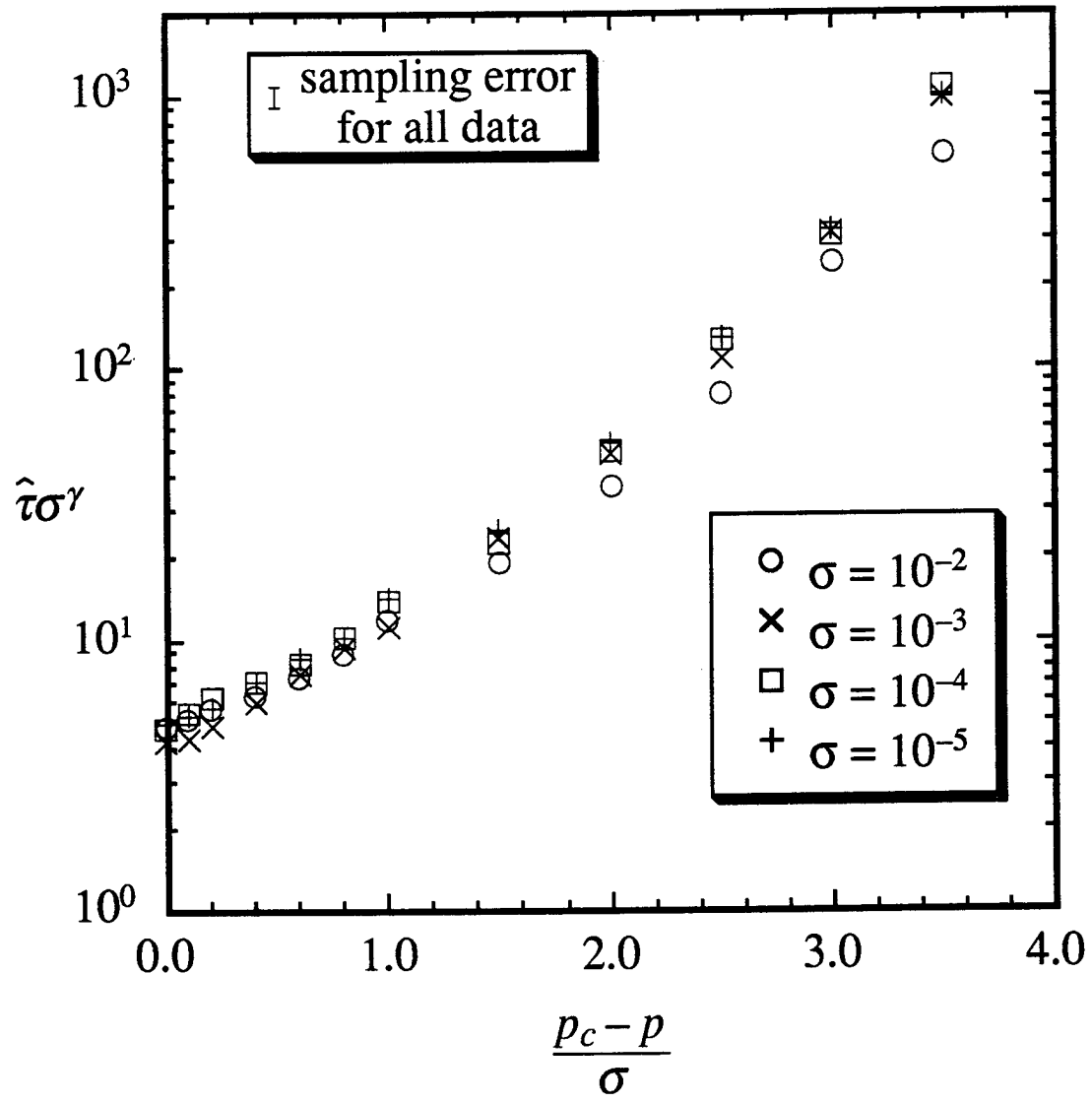

FIG. 9. Scaling form (2′) is observed for a three order-of-magnitude range of noise strength in the noisy Hénon map operated near a heteroclinic tangency crisis. $\gamma \approx 0.8557$ based on the eigenvalues of the period-1 saddle on the attractor and Eq. (4).

The non-universality of the function $g(\bullet)$ in Eq. (2) is demonstrated in Fig. 10, where the results of numerical experiments using several different noise density functions (see figure caption) are compared. Although varying σ leaves data from experiments with the same noise density along a single curve, the curves produced by the different densities have no apparent relation to one another. One way of addressing the lack of a theoretical prediction for $g(\bullet)$ in experiments is to operate the system at the parameter value corresponding to the deterministic crisis. Then Eq. (2) is restricted to a form akin to the deterministic scaling law (1), with the noise strength σ taking the role of the parameter excess p–p_c:

$$\tau \sim \sigma^{-\gamma} g(0) \sim \sigma^{-\gamma}. \qquad (2'')$$

A comparison of the numerical results from the noisy Hénon map with the restricted scaling (2″) is given in Fig. 11, where the statistical consistency again supports the applicability of Eq. (2) to this system.

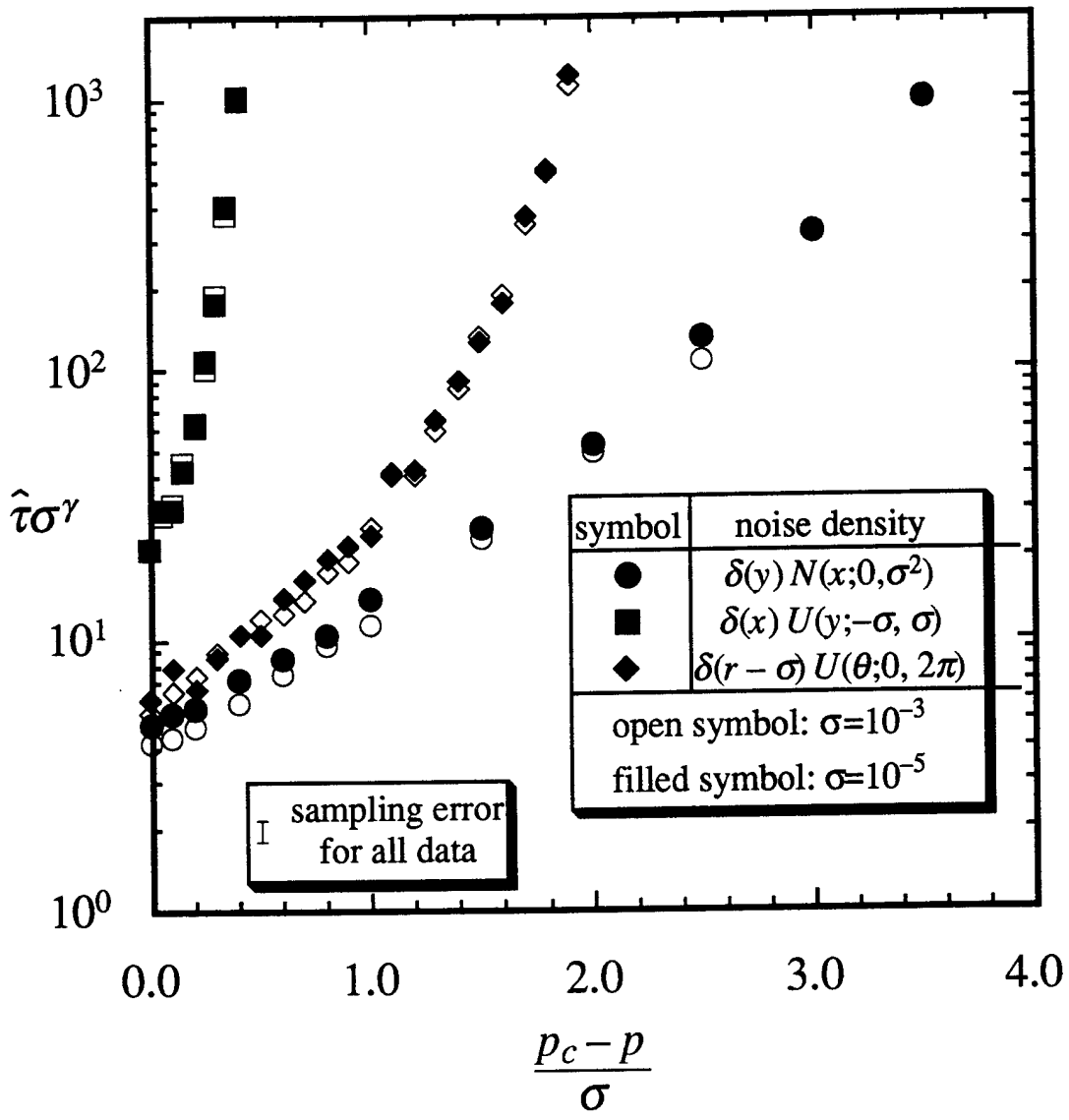

FIG. 10: Different noise densities result in different functions $g(\bullet)$ in Eq. (2), even for the same system, in this case the noisy Hénon map near the heteroclinic tangency crisis dealt with in Fig. 9. The three types of symbol each relate to a different form of the density of the additive noise; the open and closed symbols of a given type demonstrate that the scaling (2) pertains over a range of σ within each type of noise.

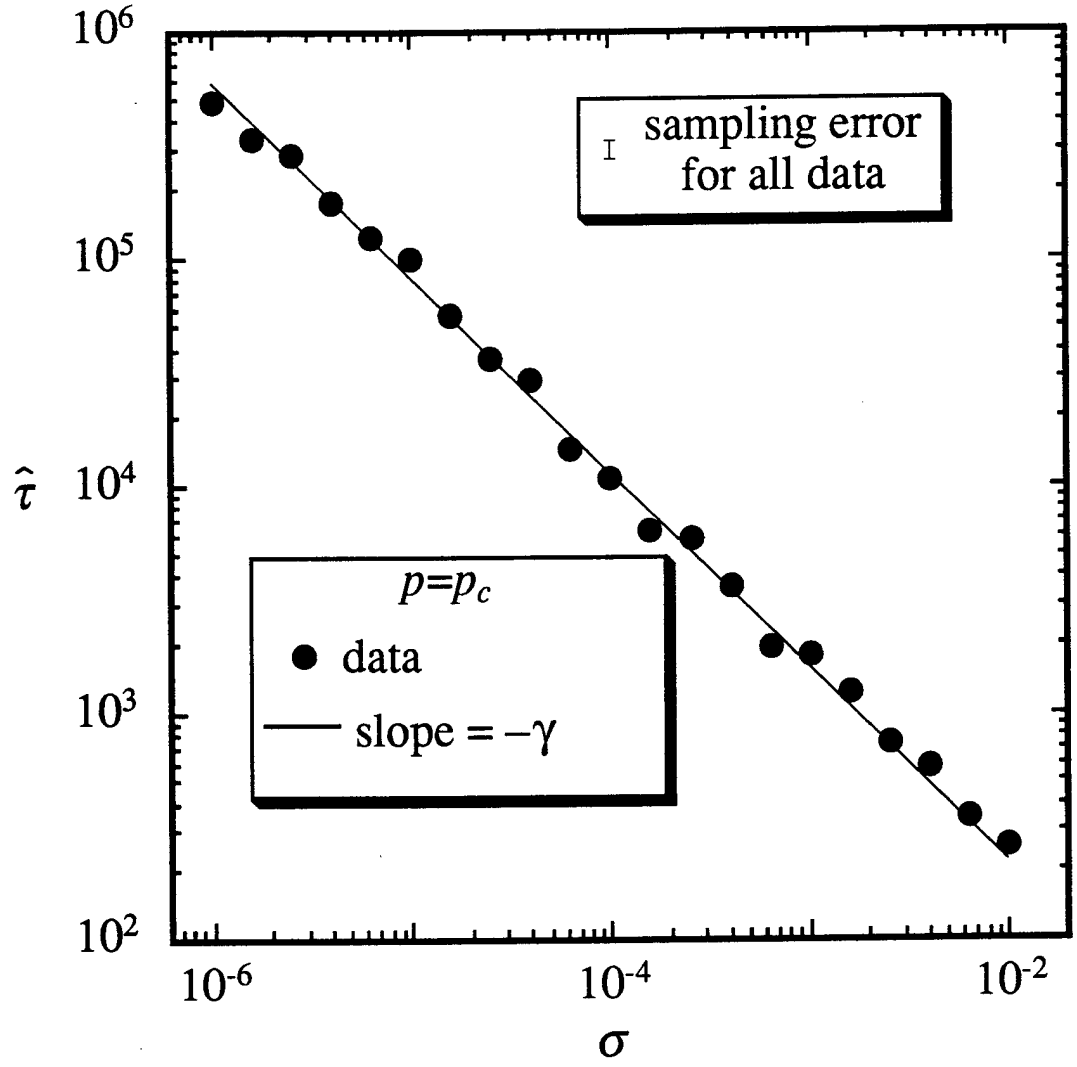

FIG. 11. Restricting $p=p_c$ fixes the argument of $g(\bullet)$ in Eq. (2), resulting in a scaling similar to Eq. (1). The slope of the straight line is $-\gamma \approx -0.8557$ based on the eigenvalues of the period-1 saddle on the attractor and Eq. (4).

B. Ikeda-Hammel-Jones-Maloney map; homoclinic tangency crisis

The Ikeda-Hammel-Jones-Maloney map, a model for a nonlinear optical ring resonator[13] was modified by additive noise to produce the system

$$w_{n+1} = A + Bw_n exp[i\kappa - i\alpha/(1+|w_n|^2)] + Z_n, \qquad (16)$$

where $w_n=x_n+iy_n$; x, y, A, B, κ, α, Z_n are all real; and Z_n are independent, identically distributed random variables with a uniform density $U(x;-\sigma,\sigma)$. For $A=A_C\approx 1.0024$, $B=0.9$, $\kappa=0.4$, and $\alpha=6.0$, the deterministic system corresponding to map (16) has a homoclinic tangency crisis mediated by an unstable fixed point (corresponding to B in Fig. 3(b)), which results in destruction of the attractor existing for $A<A_C$. (Note that in this case, A takes the role of the generic crisis parameter p.) Based on the eigenvalues of the unstable fixed point, Eq. (5) yields a critical exponent for the deterministic scaling law (1) of $\gamma\approx 1.705$. The relatively large value of the exponent γ limited the dynamic range of noise that could be investigated numerically, due to the extremely long transients obtained for smaller values of σ. (In fact, to obtain even somewhat less than three orders of magnitude variation in σ, censored sampling techniques were necessary. In censored sampling to determine a characteristic time, an ensemble of m orbits is advanced in parallel iterate by iterate. The mean lifetime is deduced statistically[14] after only the first $r<m$ orbits end their transient responses, resulting in a large computational saving relative to allowing all of the ensemble of r orbits to escape. The resulting statistical confidence is equivalent to the r out of r case. In this and the following examples, typically $r=128$, $m=256$.) Nevertheless, the results of the numerical experiments, when compared to restricted scaling form (2″) as in Fig. 12, suggest that this system also exhibits the predicted scaling.

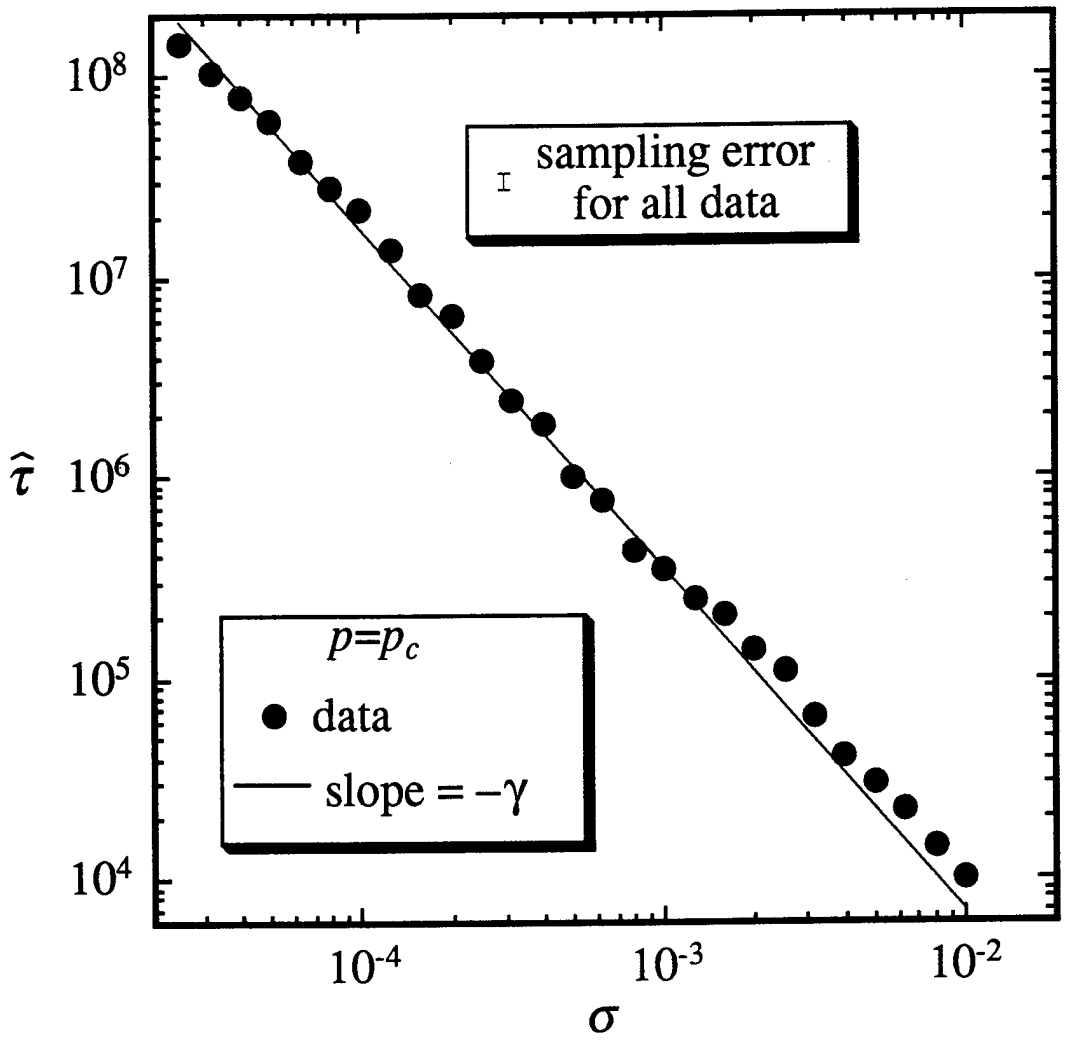

FIG. 12. The restricted scaling law (2″) is consistent with the results of this numerical experiment on the noisy Ikeda-Hammel-Jones-Maloney map near a homoclinic tangency crisis. The slope of the straight line is $-\gamma \approx -1.705$ based on the eigenvalues of the period-1 saddle mediating the crisis and Eq.(5).

V. POTENTIAL COMPLICATIONS TO OBSERVING SCALING LAW (2)

Although scaling law (2) agreed with the results of the numerical experiments on the systems discussed in the previous chapter, we have also found examples where agreement with the scaling is less immediately apparent. In this section, we discuss two such examples that illustrate problems that might be encountered in physical experiments with noisy systems. The first example (Chapter V A) shows how frequently-encountered properties of the measure of chaotic attractors, that were not explicitly addressed in the derivation in Chapter II, can lead to results that cluster around, rather than on, the curve $g(\bullet)$ in Eq. (2). The second example (Chapter V B) shows that the range of noise strengths over which scaling law (2) can be observed may be restricted. This happens when there are mechanisms, different from the tangencies of the deterministic crisis, by which the noise can cause orbits to escape.

A. Ragged measure of deterministic attractor

The analysis of Chapter II B leading to Eq. (5) for a homoclinic tangency crisis showed that the striations of the strange attractor (which has a Cantor-set structure) near its tangencies with the stable manifold of the periodic point mediating the crisis, accumulate at the geometric rate β_2, the stable eigenvalue of the periodic point B of Fig. 3(b). This means that as one considers the attractor measure as a function of distance away from one of the tangencies, measured perpendicularly relative to the stable manifold, it has a "stair-step" quality with successive steps being $1/\beta_2$ wider than the last. This effect has been observed in numerical experiments on deterministic crises. In particular, in log-log plots of τ versus $(p-p_c)$, oscillations periodic in $log_{10}(p-p_c)$ were seen to be superimposed on the logarithmically linear behavior of scaling law (1), where the period of the oscillation is[5] $log_{10}(1/\beta_2)$. For cases where $\beta_2 << 1$, this effect is particularly pronounced, and we refer to it as resulting from a *ragged* measure. In noisy

systems, a ragged measure can also complicate the observation of scaling law (2) as we now demonstrate with another numerical example based on the noisy Hénon map, Eq. (15).

For J=0.3, $p=p_c\approx$2.124 672 450 the deterministic analog of Eq. (15) undergoes a homoclinic tangency crisis mediated by an unstable period-3 orbit, which results in destruction of the chaotic attractor existing for $p\leq p_c$. The eigenvalues of the mediating saddle are $\beta_1\approx$10.9 and $\beta_2\approx$0.00247; the small stable eigenvalue leads to a pronounced periodic component in numerical results plotted as $log_{10}(\tau)$ versus $log_{10}(p-p_c)$, with period $log_{10}(1/\beta_2)\approx$2.6 (base ten) log units.[5] An analogous periodicity is noted in the results of numerical experiments intended to test the restricted scaling form (2″) on the noisy system, as shown in Fig. 13 [where the noise was $U(x;-\sigma,\sigma)$]. The oscillations superimposed on the straight-line scaling implied by Eq. (2″) have an amplitude we denote $\Delta log_{10}(\tau)$.

The observation of oscillations in the the noisy system probably depends on more than the presence of a ragged measure. In the deterministic case, a parameter excess, $p-p_c>0$, leads to fingers of the attractor remnant poking over the stable manifold (like region *ab* in Fig. 4 for the heteroclinic case) where each finger is the image under the map of the previous finger. In the deterministic case, it suffices to look at the measure in a single finger, because once an orbit crosses the stable manifold, it stays across the stable manifold on successive iterates. Therefore, as a region in one finger with a large value of $d\mu(\varepsilon)/d\varepsilon$ [corresponding to a region of higher-than-average slope on a plot of $log_{10}(\tau)$ versus $log_{10}(p-p_c)$] just crosses the stable manifold, regions of correspondingly high $d\mu(\varepsilon)/d\varepsilon$ in all the other fingers will simultaneously cross the stable manifold as well. However, the situation is different in the noisy case. For a given noise strength σ orbits can escape if they are located within a distance of order σ from the stable manifold of periodic orbit *B*.

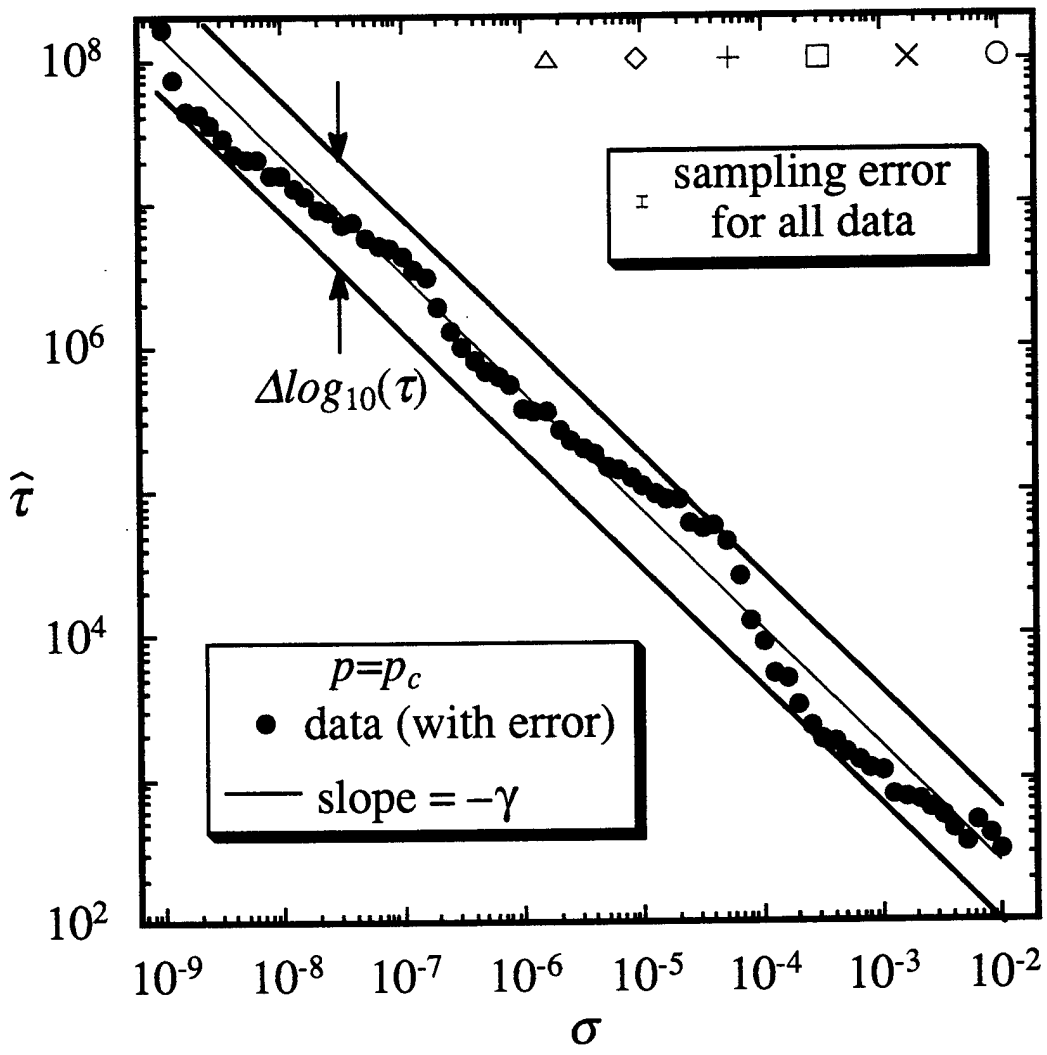

FIG. 13. Results of the numerical experiment on the noisy Hénon map near a homoclinic tangency crisis mediated by a period-3 saddle. The restricted scaling (2″) shows evidence of the raggedness of the attractor's natural measure. $log_{10}(\tau)$ has a component periodic in $log_{10}(1/\beta_2) = log_{10}(404.9\ldots) \approx 2.61$ with an amplitude of $\Delta log_{10}(\tau)$. The slope of the straight lines are $-\gamma \approx -0.83$ based on the eigenvalues of the period-3 saddle. The plot symbols at upper right indicate the values of σ for which the corresponding curves of Fig. 14 were computed.

Each finger (now analogous to region aoc in Fig. 5) represents an independent opportunity for escape. Furthermore, the region in each finger which is accessible for escape is not simply the image of the corresponding region in the previous finger. Each finger makes a contribution to the overall escape rate that is periodic in $log_{10}(\sigma)$, but the phases of these separate oscillations are different. This would tend to reduce the amplitude of any observable oscillations. However, if the measure in one finger dominates that in the others, oscillations such as those in Fig. 13 can be seen regardless of the phase relationships. Such a situation seems relatively common.

Oscillations superimposed on the restricted scaling (2″) produce even stronger effects on results relevant to the general scaling (2). Consider the effects of the ragged measure in this example for σ held constant as $p_c - p$ is increased from zero. The quantity $\tau\sigma^{\gamma}$ increases as $g(\bullet)$ increases. The starting point of the curve, the value of $g(0)$, should be obtainable from the data in Fig. 13. However, note that different values of $g(0)$ are obtained for different σ due to the oscillations about scaling law (2″). Thus, for different values of σ the quantity $\tau\sigma^{\gamma}$ should follow different, parallel curves as $(p_c - p)/\sigma$ is varied. This is essentially what is seen in Fig. 14, where the results fall in a band of approximate width $\Delta log_{10}(\tau)$, the same as the amplitude of the superimposed oscillations of Fig. 13. In general, results for σ corresponding to a trough in Fig. 13 fall in the lower part of the band in Fig. 14, while results for σ corresponding to a crest in Fig. 13 fall in the upper part of the band in Fig. 14. Obviously, if extensive data, as in Fig. 14, are not taken from a system with the properties of this example, one would have difficulty confirming the applicability of Eq. (2). This could also result in an erroneous determination of the critical exponent γ.

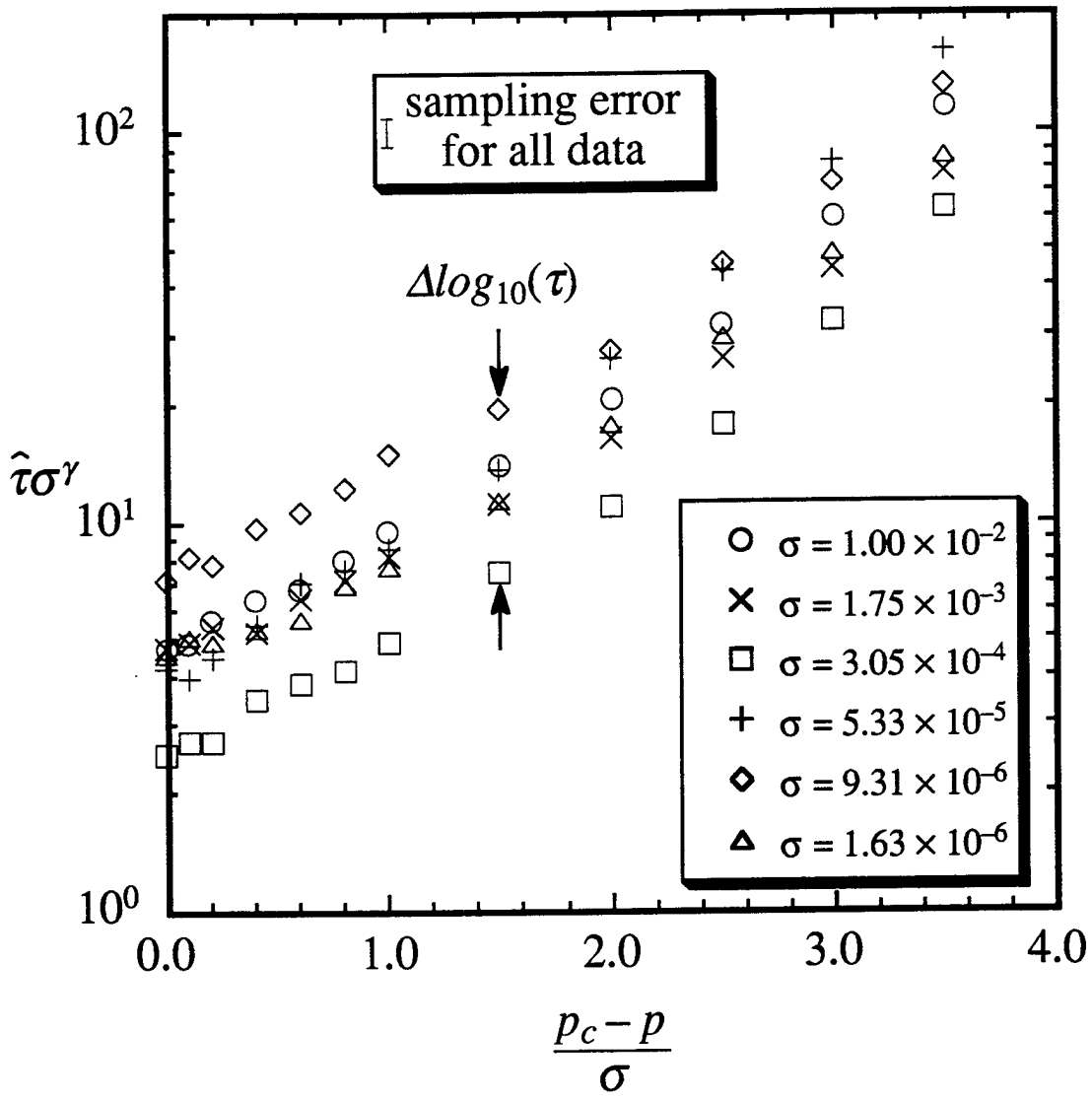

FIG. 14. The scaling (2) is obeyed only approximately for the noisy Hénon map near the homoclinic tangency crisis dealt with in Fig. 13. The results fall in a band of width $\Delta log_{10}(\tau)$, (the same as the amplitude of the wiggles in Fig. 13), rather than on a single curve.

B. Competing routes of escape

Another potentially common obstacle to observing scaling behavior (2) in physical systems is the presence of alternative routes for orbits to escape under the influence of noise, *i.e.*, routes other than the crisis-producing tangencies. We demonstrate this with another crisis of the Ikeda-Hammel-Jones-Maloney map given by Eq. (16). For A=0.85, B=0.9, κ=0.4, and $\alpha=\alpha_c\approx$7.268 849, the deterministic system corresponding to map (16) has a heteroclinic tangency crisis mediated by an unstable period-5 orbit, which results in crisis-induced intermittency known[5] to conform to Eq. (1) for $\alpha>\alpha_c$ (in this case α, rather than A, takes the place of the generic crisis parameter p). The results of numerical experiments intended to confirm the applicability of restricted scaling law (2″) for the noisy map [the noise was again $U(x;-\sigma,\sigma)$] are shown in Fig. 15. The fit to the predicted exponent γ is only good for very small σ ($\sigma<10^{-3}$).

The reason for this failure is shown schematically in Fig. 16. The stable manifold colliding with the chaotic attractor makes a number of close approaches to the chaotic attractor that nevertheless do not become tangencies for $p=p_c$. These close approaches, although having no effect on the observability of scaling law (1) for the deterministic system, provide an additional route of escape for the noisy trajectories, at larger values of σ, which was not accounted for in deriving Eq. (2). Therefore, at large values of σ the observed rate of escape has two contributions, one from the crisis-producing tangencies and one from the close approaches of the stable manifold, resulting in a smaller-than-expected value of τ. For small values of σ, the close approaches do not contribute to the rate of escape, and τ conforms to Eq. (2″). Of course, it is not at all surprising that a given system will have an upper bound on σ for Eq. (2) to apply, but competing routes of escape make that bound more stringent than it would otherwise be, and provide a potential pitfall in the experimental determination of critical exponents of noise-induced crises.

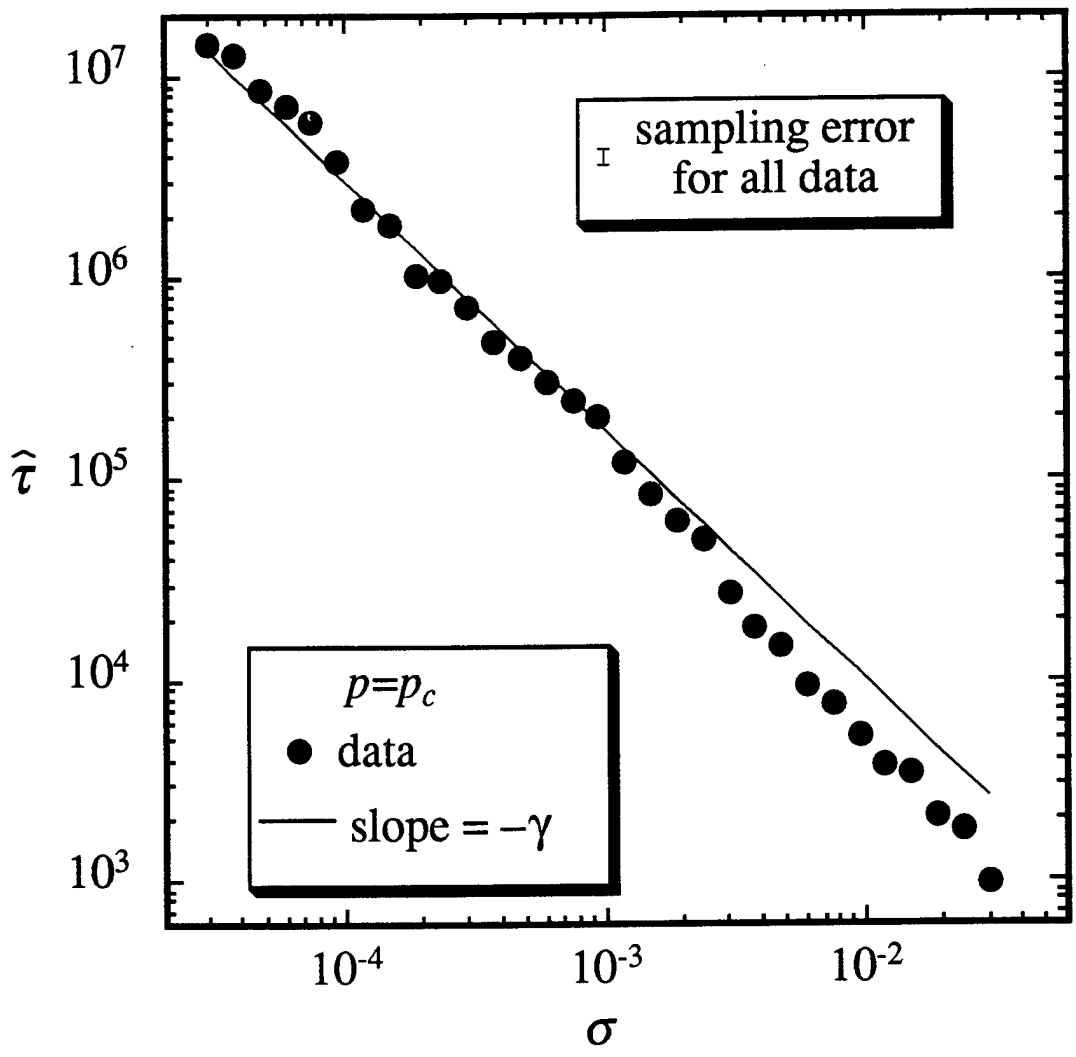

FIG. 15. The restricted scaling (2″) is violated for large σ (*i.e.*, $\sigma > \sim 10^{-3}$) in this numerical experiment with the noisy Ikeda-Hammel-Jones-Maloney map near a heteroclinic tangency crisis mediated by a period-5 saddle. The slope of the straight line is $-\gamma \approx -1.236$ based on the eigenvalues of the period-5 saddle on the attractor and Eq. (4).

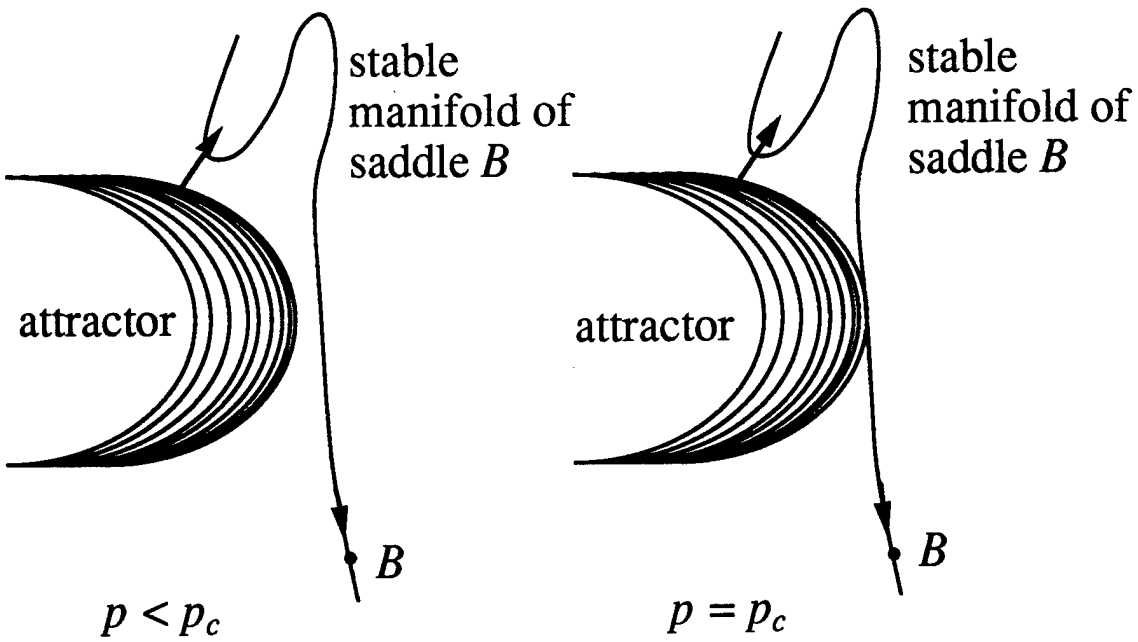

FIG. 16. Schematic of a "near tangency" unrelated to the crisis-producing tangency. The arrows indicate a route for noisy trajectories to escape that is not accounted for in the derivation of Eq. (2). Thus, for large σ an additional rate of escape will decrease τ from what is predicted on the basis of the crisis alone.

VI. APPLICABILITY OF SCALING LAW (2) TO FLOWS

Thus far, we have been rather arbitrary in adding noise to the example systems, and have ignored how noise terms might arise physically. In particular, the noise densities have been assumed to be independent of phase-space position. Although it is possible to imagine physical systems for which a discrete map is explicitly derivable from first principles (the Ikeda-Hammel-Jones-Maloney map is one example), and where noise might appear in this relatively benign fashion, in general we expect a more complicated situation. Indeed, much of the justification for studying discrete maps is that they can be viewed as occurring in a Poincaré section of the higher-dimensional phase space of a flow. However, noisy flows modeling physical systems will in general not reduce, in Poincaré sections, to noisy maps of the type seen in the examples so far. In particular, the noise applied to such a model to model the physical system will, in general, not be simply additive nor will it be independent of the coordinates in the surface of section. In this chapter we present an example of a noisy flow that is physically well-motivated, and use it to suggest that Eq. (2) is also applicable to the more realistic situation where the density function of the noise in a noisy map depends on phase-space position.

We consider a noisy version of the Duffing oscillator, a model for the one-dimensional motion of a point particle in a potential $V(x)$, which is subjected to friction, an external sinusoidal force, and random forcing like that producing Brownian motion. This situation is described by the stochastic differential equation

$$d^2x/dt^2 = -\nu\, dx/dt - dV/dx + p\, sin(\omega t) + \xi(t), \qquad (17)$$

where $\xi(t)$ is Gaussian white noise with intensity σ, *i.e.*, $\langle \xi(t)\xi(t') \rangle = \sigma^2 \delta(t-t')$. We take $V(x) = \alpha x^4/4 - \beta x^2/2$, ν=1, α=100, β=10, ω=3.5 and p near $p_c \approx 0.845$. The potential well has two minima at $x = \pm\sqrt{\beta/\alpha}$. For $p<p_c$, the deterministic analog of Eq. (17) has two symmetrically disposed chaotic attractors, one confined to the well in $x<0$ and the other to the well in $x>0$. For $p>p_c$, there is one chaotic attractor, and orbits intermittently switch

from one well to the other.[15] When considered in the $t=2n\pi/\omega$ Poincaré section, the deterministic system undergoes a homoclinic tangency crisis mediated by an unstable period-3 orbit, which results in attractor merging. Numerical experiments confirm that the crisis scaling (1) applies to this system.[5(1986)]

One of the deterministic attractors for $p<p_c$ is shown in Fig 17(a). When the stochastic system of Eq. (17) is integrated as discussed in Appendix B, the envelope of the orbit spreads out under the influence of the noise, as shown in Fig. 17(b). Note that because the noise does not appear in the argument of the sine in Eq. (17), the stroboscopic section is still a valid Poincaré section for the stochastic flow. The difference between this example and previous ones in this dissertation (which also produced "fuzzy" attractors) is best shown by considering the conditional density of trajectories under one period of the forcing, given a specified initial condition, for many different realizations of the noise; two such conditional densities are illustrated in Figs. 17 (c) and (d). We see that the effect of the noise $\xi(t)$ is different in different parts of the phase space, depending on the local stretching and dissipation given by the deterministic terms in Eq. (17), resulting in a spatially-dependent density for the noise in the Poincaré section. The conditional density in the Poincaré section tends to extend along the unstable manifold of the deterministic attractor. Although the exact shape of the density is phase-space-dependent, the characteristic spread of the noise in the Poincaré section is of the same order over the region of the deterministic attractor, and that characteristic spread scales linearly with the noise intensity parameter σ. Therefore, it seems reasonable to try to apply scaling law (2) to this and other continuous-time systems.

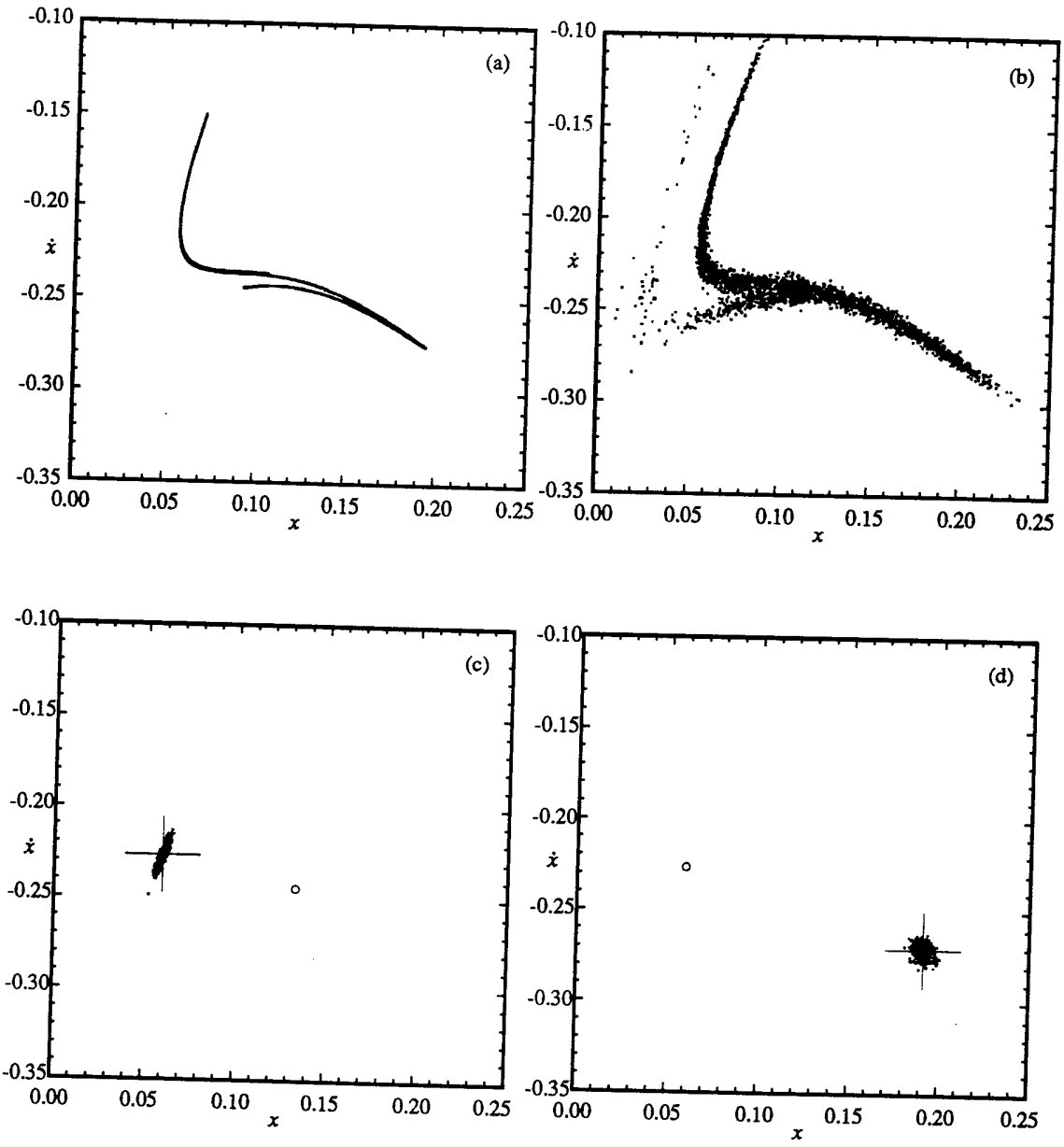

FIG. 17. (a) One of the two $p<p_c$ attractors of the deterministic differential equation (17), shown in the $t=2n\pi/\omega$ Poincaré section. 5000 iterates of a trajectory are plotted. (b) The noisy attractor for $\sigma=10^{-5}$. Again, 5000 iterates were computed, but a number of transitions between the $x<0$ and $x>0$ potential wells have already taken place, due to the nearby (in parameter space) homoclinic tangency crisis. (c) and (d) Conditional densities of the trajectory after one forcing period, given an initial condition. The stochastic differential equation was integrated for one forcing period for 800 different noise realizations, starting from the initial condition shown by the circle. The deterministic trajectory is shown by the cross. The noise density in the Poincaré section is clearly space-dependent.

Figures 18 and 19 show that scaling law (2), with γ determined from the eigenvalues of the period-3 orbit, does indeed apply to the stochastic differential equation (17), albeit with the complications discussed in Chapter V A, which are unrelated to the fact that the system is a flow, rather than a map. Here, the scale of the oscillations superimposed on restricted scaling form (2″) is particularly large, because the stable eigenvalue of the mediating period-3 saddle in the Poincaré section is so small ($\beta_2 \approx 0.000512$).

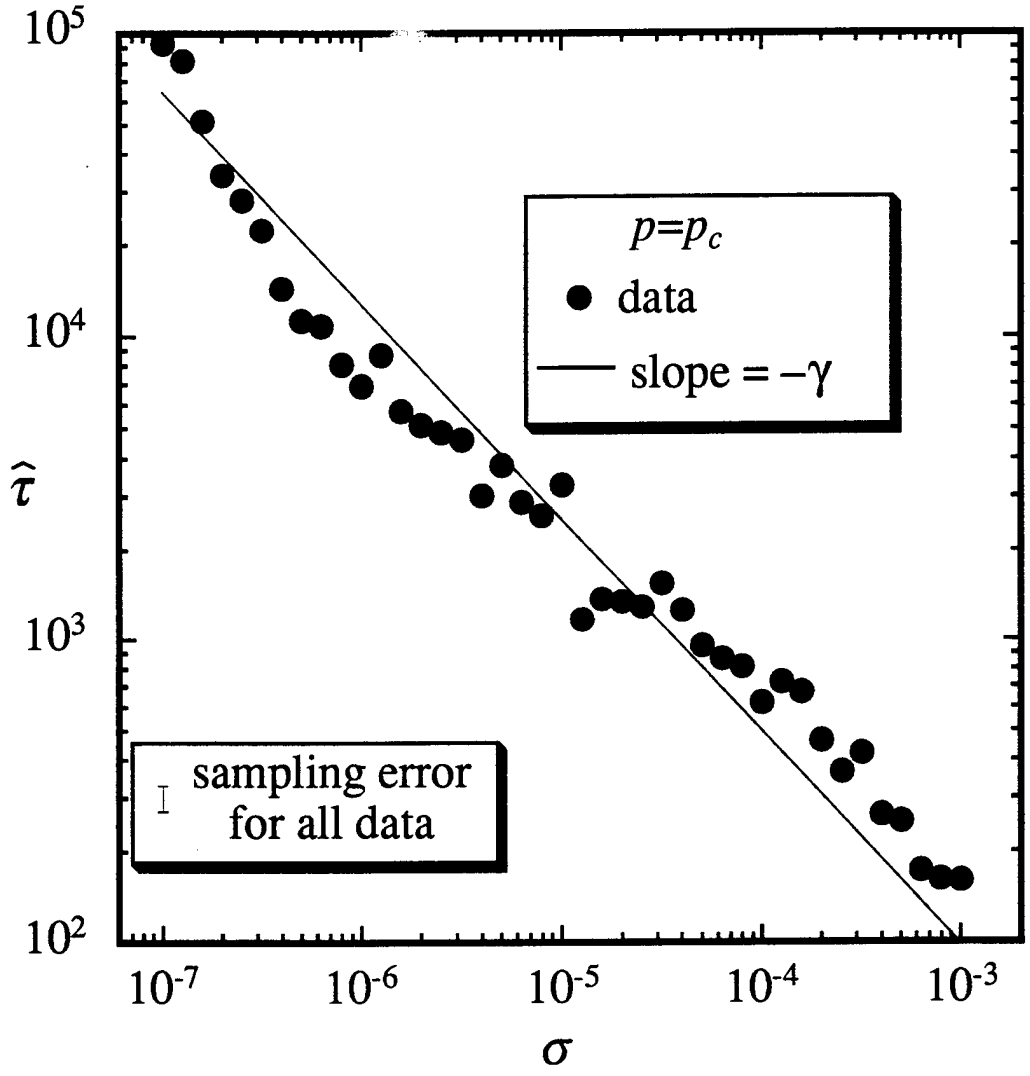

FIG. 18. The restricted scaling (2″) applies to the stochastic differential equation (17), with the same type of measure-dependent structure seen in Fig. 13. The scale of variation is larger here because the stable eigenvalue of the mediating period-3 saddle in the Poincaré section is so small ($\beta_2 \approx 0.000512$). The slope of the straight line is $-\gamma \approx -0.703$ based on the eigenvalues of the period-3 saddle.

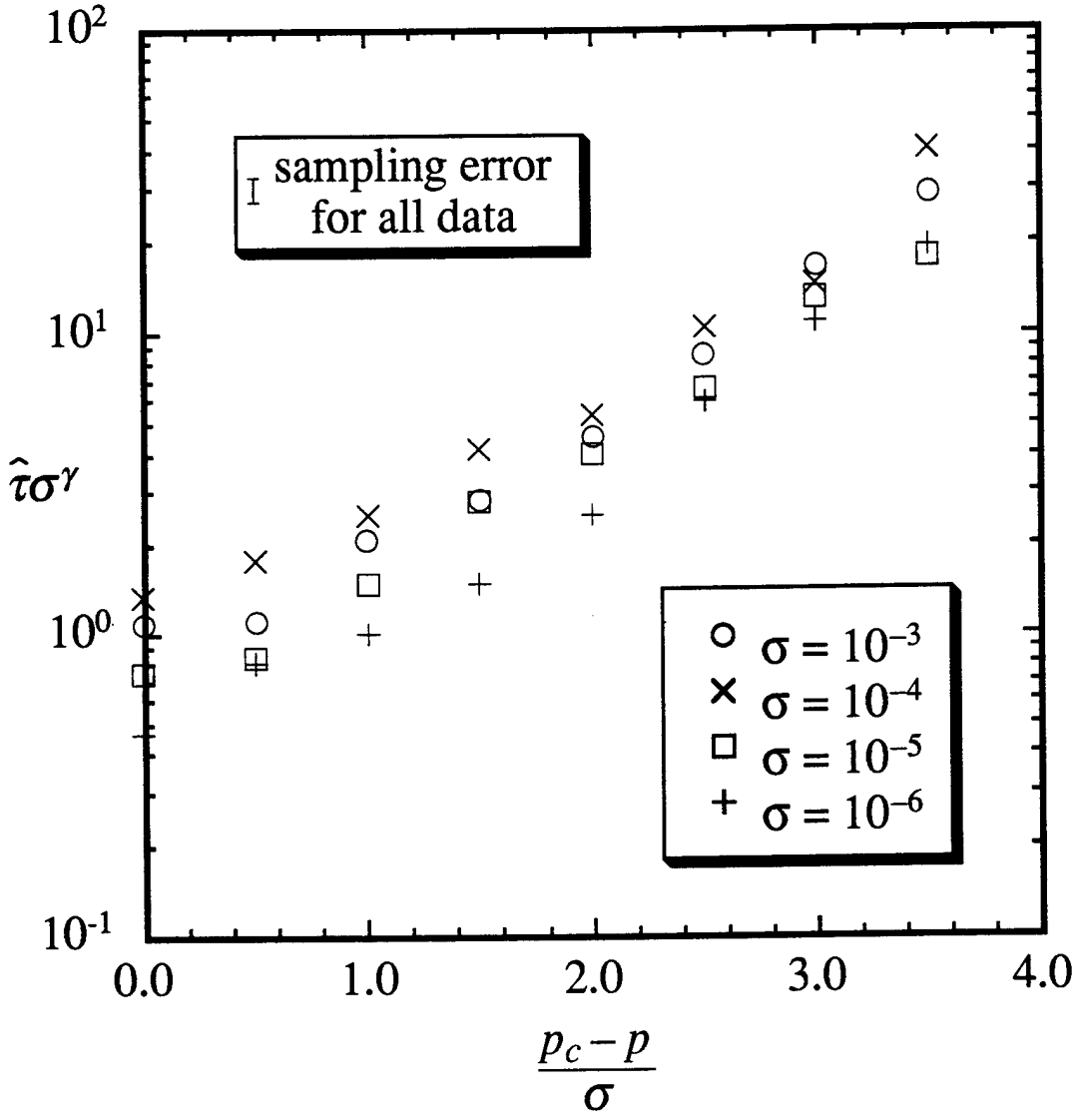

FIG. 19. The scaling (2′) applied to the results of the numerical experiment with the stochastic differential equation (17). The scaling curve $g(\bullet)$ is broadened as in Fig. 14.

VII. IMPLICATIONS FOR EXPERIMENTS

In this chapter, we summarize the implications of scaling law (2) for experiments on physical systems accompanied by noise. These implications are intrinsic to noisy systems, and are not merely special (although common) problems like those discussed in Chapter V. Figure 20 shows in three-dimensional form the qualitative dependence of the characteristic time τ of noise-induced crises on the strength of the noise σ and the parameter p. Note that the region $p>p_c$ is also included in the figure. The derivation in Chapter II did not explicitly address the case of $p>p_c$, but our experience with numerical experiments confirms the reasonable idea that for noisy systems with $(p_c - p)/\sigma$ small and negative, the behavior is continuous with that for $(p_c - p)/\sigma$ small and positive; for $(p_c - p)/\sigma$ large and negative, the system behaves as in a deterministic crisis.

A typical experiment is to determine the parameter value at which a crisis occurs, by measuring the length of the transient as a function of the parameter. Ideally, one should do this in a vertical plane $\sigma=0$ of Fig. 20, where τ would go asymptotically to infinity at $p=p_c$. However, the presence of noise limits the experiment, at best, to some vertical plane $\sigma\neq0$, where large values of τ are found for $p<p_c$. Thus, there is a tendency for p_c to be underestimated in systems with noise, and for the system to appear to disobey the deterministic scaling law (1) for $p–p_c$ varied over a wide dynamic range.

If an underestimate of p_c from experiments on a supposedly deterministic system is used in a subsequent experiment where additional noise is intentionally added, as a probe, to test the applicability of scaling law (2), spurious results will again be possible. For example, a test of Eq. (2″) should ideally take place in the vertical plane $p_c - p = 0$ of Fig. 20, where intersection with the surface yields a straight line for $ln(\tau)$ versus $ln(\sigma)$. The previous underestimate of p_c will lead to the experiment being done in a vertical plane $p_c - p > 0$, where the $ln(\tau)$ versus relation $ln(\sigma)$ will be nonlinear.

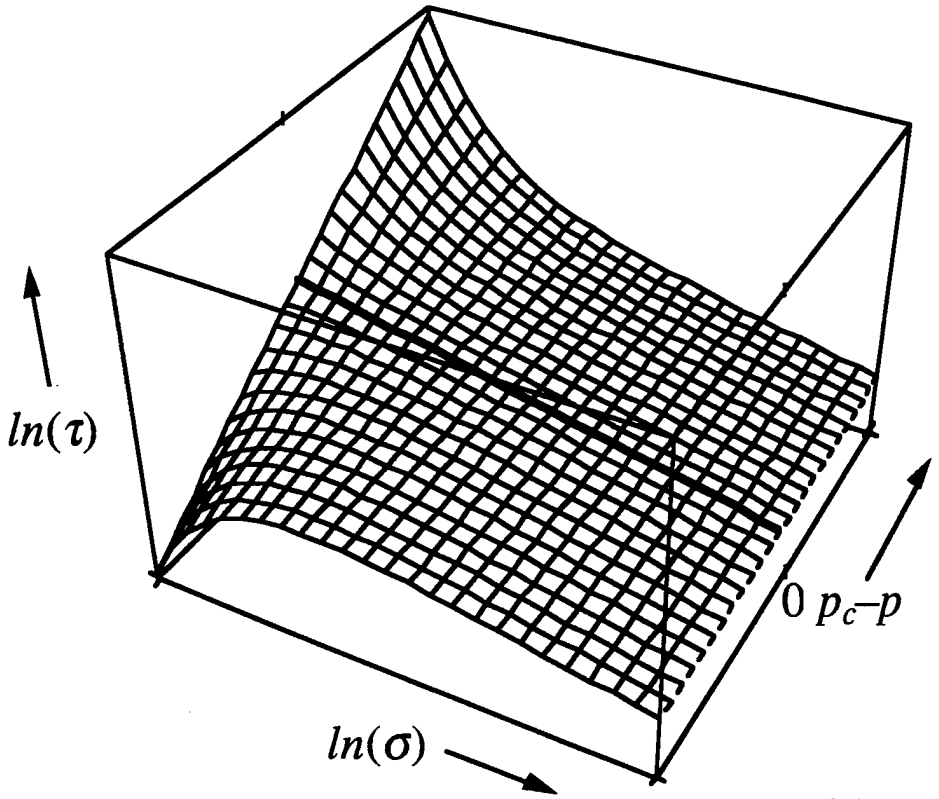

FIG. 20. The surface displays the parameter and noise dependence of the transient length for a notional scaling function $g(\bullet)$. The thick line gives the restricted scaling (2″). Curves in vertical planes parallel to the thick line correspond to attempts to observe the restricted scaling with an error in p_c. Vertical cuts of the surface by planes σ=const give the results of parameter variation in a noise-limited experimental system.

Obviously, the experimental difficulty associated with the problems mentioned here will depend on the particular system. Problems will be minimized if the dynamic range of added noise is maximized and well above intrinsic noise levels (for example, in the numerical experiments, noise was present in the form of roundoff error, but its strength was separated by many orders of magnitude from that of the added noise). This requirement may conflict with the avoidance of potential problems like those discussed in Chapter V B, where the global properties of the system place an upper bound on the noise strength that can be meaningfully applied.

VIII. EXPERIMENTAL CONFIRMATION OF SCALING LAWS (1) AND (2)

In this chapter, we present the results of physical experiments that confirm the applicability of scaling laws (1) and (2) to physical systems. We have observed crisis-induced intermittency in a variable-noise, nonlinear mechanical system, and have for the first time confirmed the theoretically-predicted key role played by an unstable orbit in mediating a deterministic crisis. We identify the unstable periodic orbit mediating the crisis and compare the critical exponent predicted on the basis of the orbit's eigenvalues with the scaling behavior of the time between bursts, τ. We find good agreement between the predicted and measured exponents.

We have also observed *noise-induced* intermittent bursts in the nonlinear mechanical system for $p<p_c$, and have confirmed experimentally the applicability of scaling law (2) to a physical system. We calculate the critical exponent γ for the $p>p_c$ system, using three operationally independent means that produce results in good agreement, and show that the characteristic time for the $p<p_c$ system is consistent with a single function $g(\bullet)$ over a wide range of σ and $p-p_c$, when γ is used to scale the results as in Eq. (2).

In Section A, we discuss the experimental setup and the measurements made on the nonlinear mechanical system. In Section B, we discuss the results obtained by operating the system with the variable noise turned off, which are relevant to the theory of deterministic crises leading to Eq. (1). In Section C, we discuss the results obtained by adding noise to the system.

A. Experimental Setup and Procedures

The experimental system was a gravitationally buckled, amorphous, magnetoelastic ribbon[16] (transversely annealed $Fe_{81}B_{13.5}Si_{3.5}C_2$; 3mm x 65mm x 25$\mu$m), clamped vertically at its base, and driven parametrically by a time-varying

component to an applied magnetic field (Fig. 21). The time-varying component had both a sinusoidal and a random contribution. The random component was given by

$$\xi(t) = \sum_{k=-\infty}^{\infty} a_k \left\{ \theta(t - k\,\delta t) - \theta[t - (k+1)\,\delta t] \right\},$$

where $\theta(\bullet)$ is the unit step function, δt is an update interval much smaller than both the mechanical response time of the ribbon and the forcing period, and the a_k are independent, zero-mean Gaussian random variables with variance σ_a^2. This form approximated Gaussian white noise. The ribbon is made from a new class of amorphous materials that exhibit very large reversible changes in their Young's modulus E with the application of a small magnetic field (inset, Fig. 21). The oscillating magnetic field changes the stiffness of the ribbon, which therefore buckles to a correspondingly greater or lesser degree. It should be noted that although the variable noise appears additively in the magnetic field, the ribbon experiences *parametric* noise; thus, the applicability of the theory leading to Eq. (2) is not immediately guaranteed. The degree to which the ribbon is buckled is measured by an MTI Fotonic sensor near the base of the ribbon. Additional details of the apparatus are discussed in Ref. 17. The sensor output, monotonically related to the ribbon curvature, was used as the single measured dynamical variable in the experiments. The rest of the system's phase portrait was reconstructed by delay-coordinate embedding.[18] The sensor output voltage time series was $V_i = V(t_i)$ ($t_i = i\Delta t$; i=1, 2, 3...; $\Delta t = 1/f$, the forcing period). This choice of Δt was made to obtain a stroboscopic Poincaré section in a (d+1)-dimensional continuous-time phase space. For sufficiently large d, this choice of Δt induces a discrete d-dimensional map $\mathbf{x}_{i+1} = \mathbf{F}(\mathbf{x}_i)$ for the system, where $\mathbf{x}_i = (V_i, V_{i+1}, V_{i+2}, \ldots V_{i+d})$. It should be noted that a complete model of the ribbon's behavior requires a partial differential (*i.e.*, infinite-dimensional) equation. It is therefore noteworthy that essential features of the ribbon's dynamics can be captured in a low-dimensional mapping, as has been shown previously.[17,19]

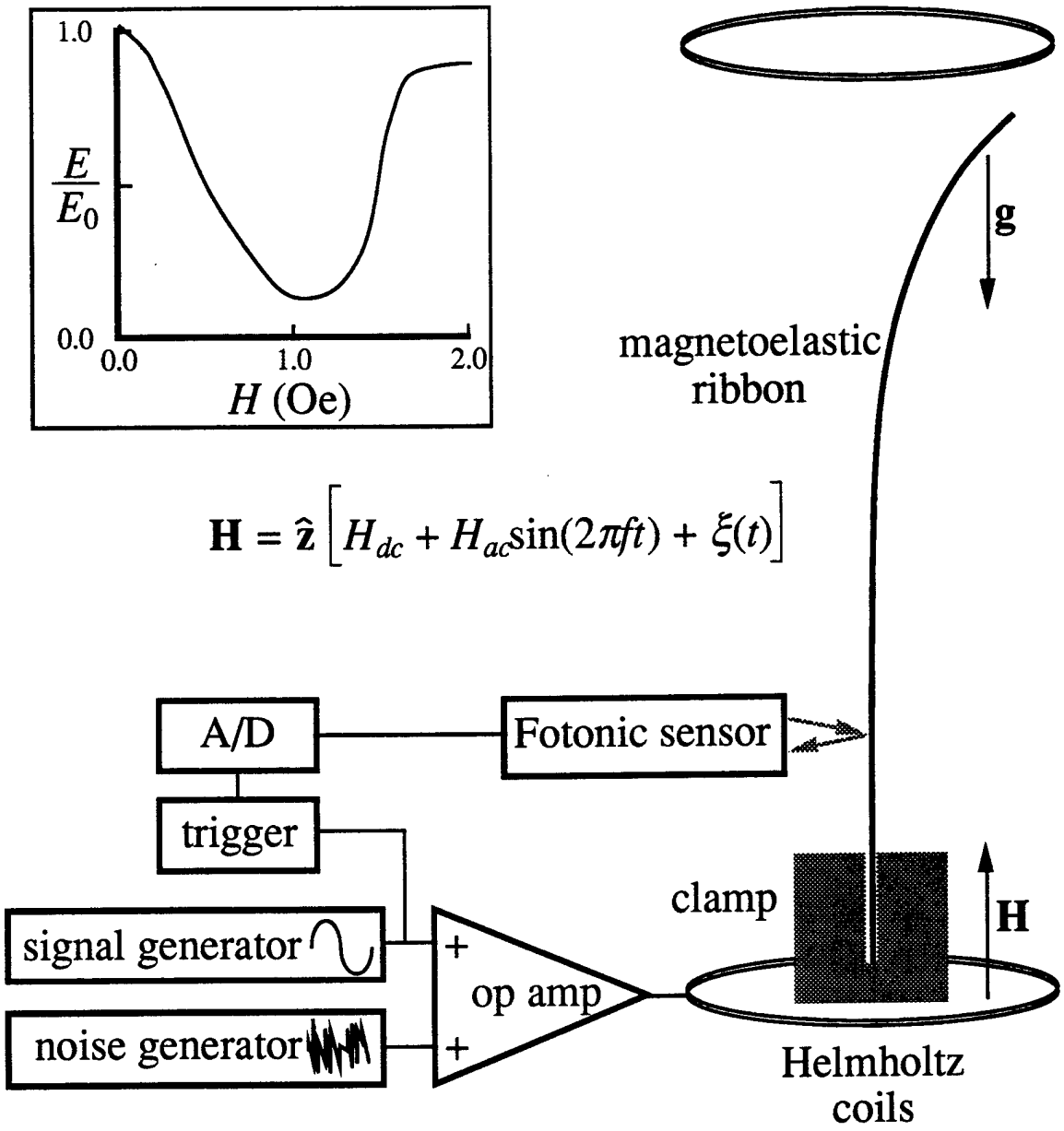

FIG. 21. Experimental setup. Inset: ratio of Young's modulus E of the ribbon to zero-field modulus E_0, vs applied magnetic field.

We observed that for an imposed magnetic field $H = H_{dc} + H_{ac}\sin(2\pi ft)$, (where H_{dc} = 0.82 Oe and H_{ac} = 2.05 Oe), as f decreases through about 0.97 Hz, the "deterministic" ($\xi \equiv 0$) system undergoes a crisis. [It is important to note that the crisis occurs as *f decreases* through its critical value, which is the opposite of the *convention* for the generic crisis parameter p used previously in this dissertation and in many of the references. To minimize confusion, we use f explicitly, rather than p in this chapter.] Before the crisis, the system state moves chaotically on a strange attractor [Fig. 22(a)]. After the crisis [Fig. 22(b)], the attractor is much larger. The dynamics during the bursts is more complicated than that between bursts. However, the part of the attractor corresponding to the pre-crisis attractor (the *core*) is adequately represented in a two-dimensional phase space, and so we expect the theory leading to Eqs. (4) and (5) to apply. Turning on the noise term ($\xi \neq 0$) produces orbits much like those of the post-crisis system, even for $f > f_c$ [Fig. 22(c)].

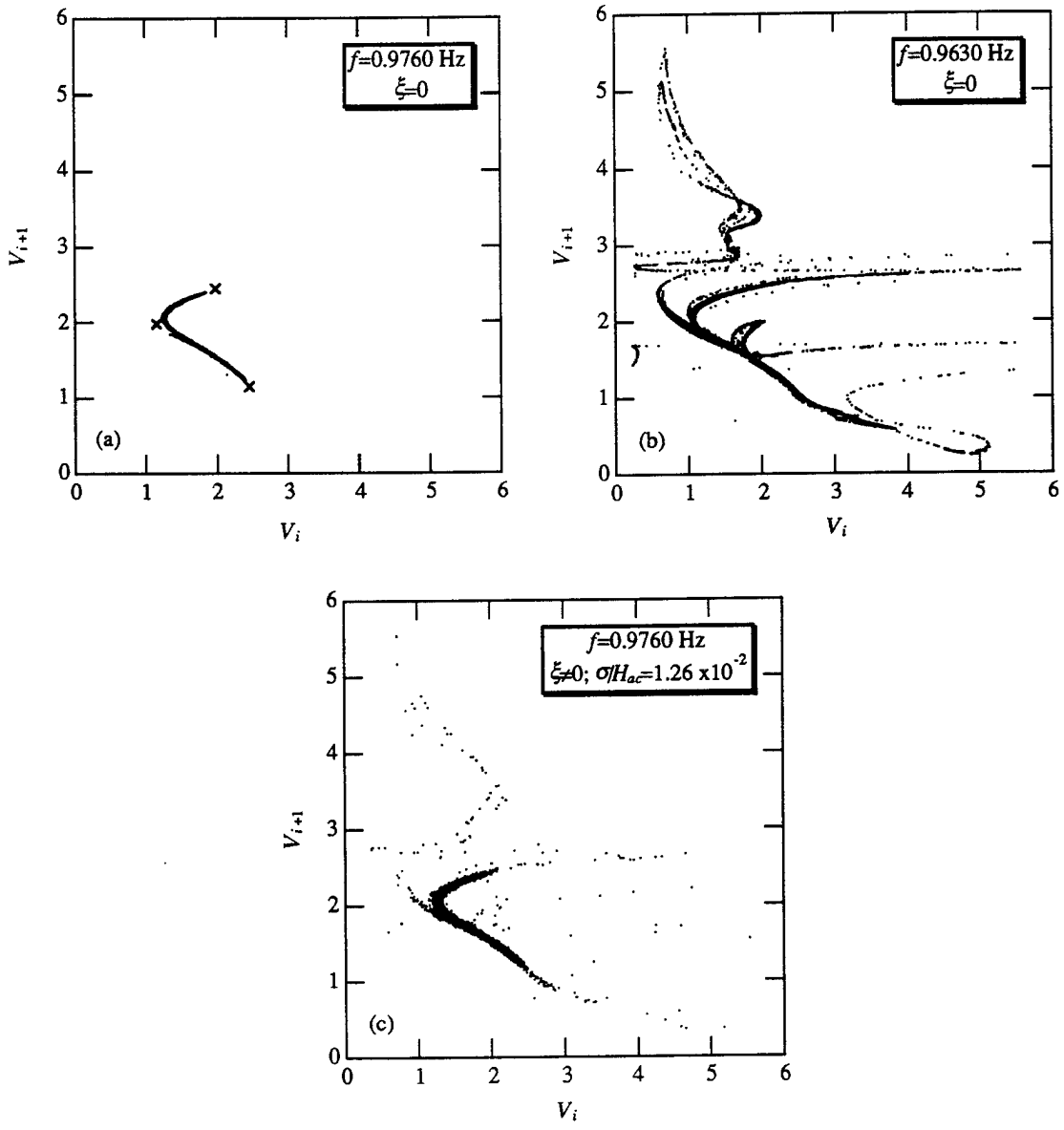

FIG. 22. Delay coordinate embedding of time series taken before (a) and after (b) the crisis. The time delay Δt is $1/f$, the stroboscopic sampling period. The core attractor of (a) is enlarged by burst dynamics in (b). In (c), the parameter is held at the same value as in (a), but the variable noise is on. The noise produces burst dynamics similar to those seen in (b). The small crosses in (a) indicate the elements of the period-3 unstable orbit that mediates this crisis.

B. Analysis of Deterministic Crisis

The scaling exponent γ of the deterministic crisis was calculated in three operationally independent ways. First, γ was determined by measuring the characteristic time between bursts τ as a function of f–f_c, and fitting the results to Eq. (1). Estimates $\hat{\tau}$ of τ were obtained from 3-hour time series recorded for closely spaced values of f near the crisis ($\hat{\tau}$ is measured in forcing periods of the sinusoidal magnetic field component). The theoretical scaling law (1) for τ assumes that the system is deterministic; for such a system, the characteristic time goes to infinity at the crisis. Real systems, which are always accompanied by noise, show a finite characteristic time at f=f_c as is evident from Eq. (2). The presence of residual system noise, even with the a_i set to zero, made determining the value of f_c more complicated than in an ideal system, and somewhat limited the accuracy with which it could be determined. The value of f_c for this crisis was determined by minimizing the degree to which a plot of $\hat{\tau}$ vs $\log(f_c–f)$ deviated from a straight line, using data taken not too near f_c [where noise more strongly affects the applicability of Eq. (1)]. Given f_c, γ was determined from the best nonlinear least-squares fit of the functional form $\hat{\tau} = k(f_c–f)^{-\gamma}$ to the data. The data and corresponding fit are shown in Fig. 23. The statistical estimate of the critical exponent using this method is γ= 1.12±0.02.

A second determination of γ was made by considering the accumulation of probability measure at the edge of the attractor. The theory leading to scaling law (1) assumes[5] that the measure μ of the attractor within ε of its edge accumulates as $\mu(\varepsilon) \sim \varepsilon^{\gamma}$. Using a trajectory of several hours duration recorded for f just above f_c, the iterates were sorted in magnitude, and an estimate of $\mu(\varepsilon)$ was obtained as a cumulative count of the number of iterates within ε of the maximum iterate. The slope of the straight-line portion of a plot of $\ln[\mu(\varepsilon)]$ vs $\ln(\varepsilon)$ produced an estimate of γ= 1.08±0.05, which is statistically consistent with the above estimate.

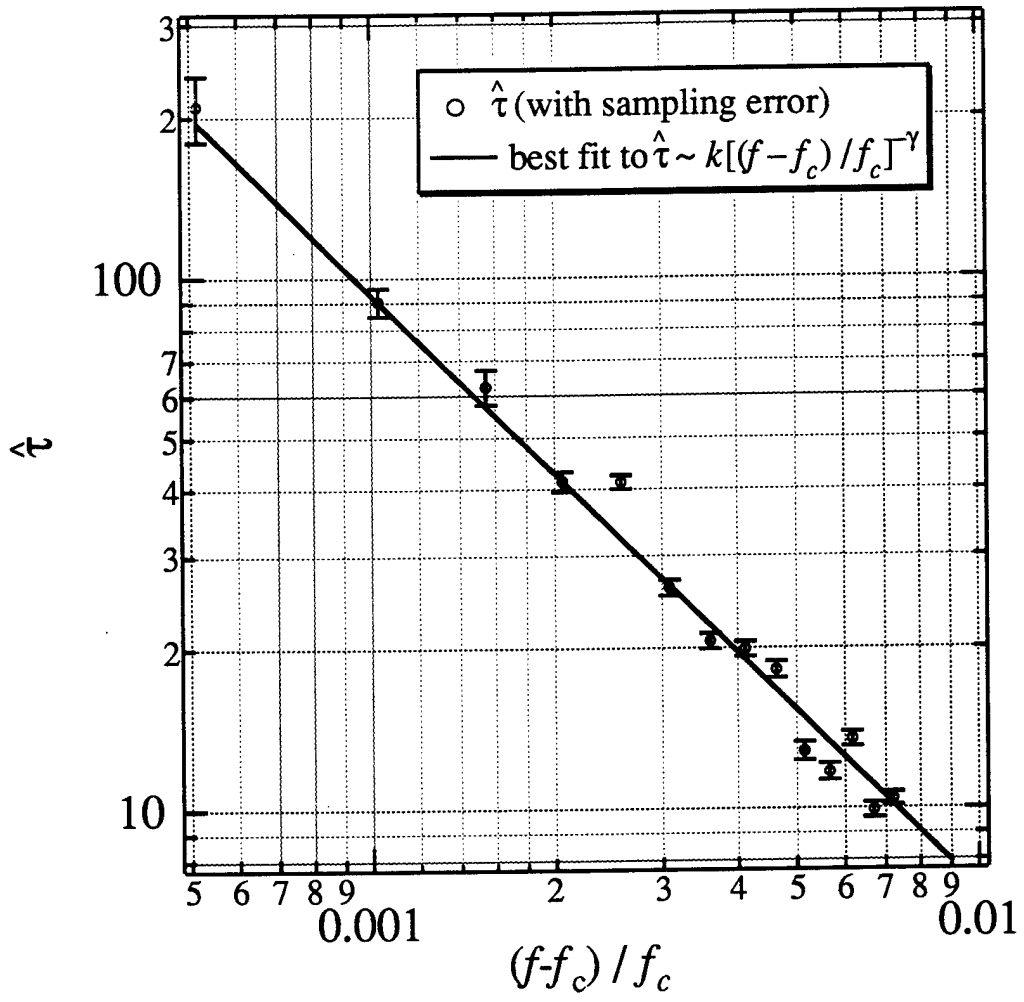

FIG. 23. Estimated mean time between bursts $\hat{\tau}$ vs $|f_c-f|/f_c$. Nonlinear least-squares fit to $\hat{\tau} = k[(f_c-f)/f_c.]^{-\gamma}$ gives $\gamma = 1.12 \pm 0.02$.

A final determination of γ resulted from the observation that the crisis shown in Fig. 22 is a homoclinic tangency crisis of a two-dimensional map. Careful observation of the system state just before a burst indicated that system trajectories closely approached a period-3 orbit [the elements of which are indicated in Fig. 22(a)] before leaving the core attractor. Figure 24 shows V_{i+3} vs V_i for the phase-space region of the core attractor after crisis; several iterates passing near the saddle are indicated. Any period-three orbit appears as fixed points of the three-times-iterated mapping $\mathbf{F}^{(3)}$ and, because we use a delay-coordinate embedding, these must lie along the 45° line (*i.e.*, $V_{i+3} = V_i$). The attractor intersects the 45° line in four places. One of these intersections is a period-1 point; the other three are elements of the same period-3 saddle. For $f>f_c$ (before the crisis), the attractor only intersects the 45° line at the period-1 point. This indicates the absence of any period-3 orbits on the attractor before crisis. Crises in two-dimensional maps are limited to two varieties, depending on whether the mediating periodic orbit is on the attractor before (heteroclinic), or only just at and after (homoclinic) the crisis.[5] The absence of a period-3 orbit on the attractor before the crisis means that the crisis is of the homoclinic type. The theoretically predicted critical exponent for this crisis should therefore be given in terms of the eigenvalues of the period-3 orbit by Eq. (5).

Estimating these eigenvalues from the experimental data is complicated by the facts that: (*i*) the map **F** is clearly very dissipative, (*ii*) the system is contaminated by noise, and (*iii*) the linear neighborhood of the period-3 point is relatively small. Therefore, following an orbit as it passes near the period-3 point, as suggested in Ref. 5, is not a good way to estimate the eigenvalues. Instead, we use pairs of iterates to estimate the Jacobian matrix of the map around the period-3 point, and from this estimate obtain the linearized eigenvalues of the periodic point [see Appendix C]. The estimate of the critical exponent based on these eigenvalues of the period-3 saddle, $\gamma = 1.07 \pm 0.15$, clearly is statistically consistent with the exponents determined independently above. Such

consistency strongly supports the key role played by unstable periodic points in mediating crisis phenomena in nonlinear dynamical systems.

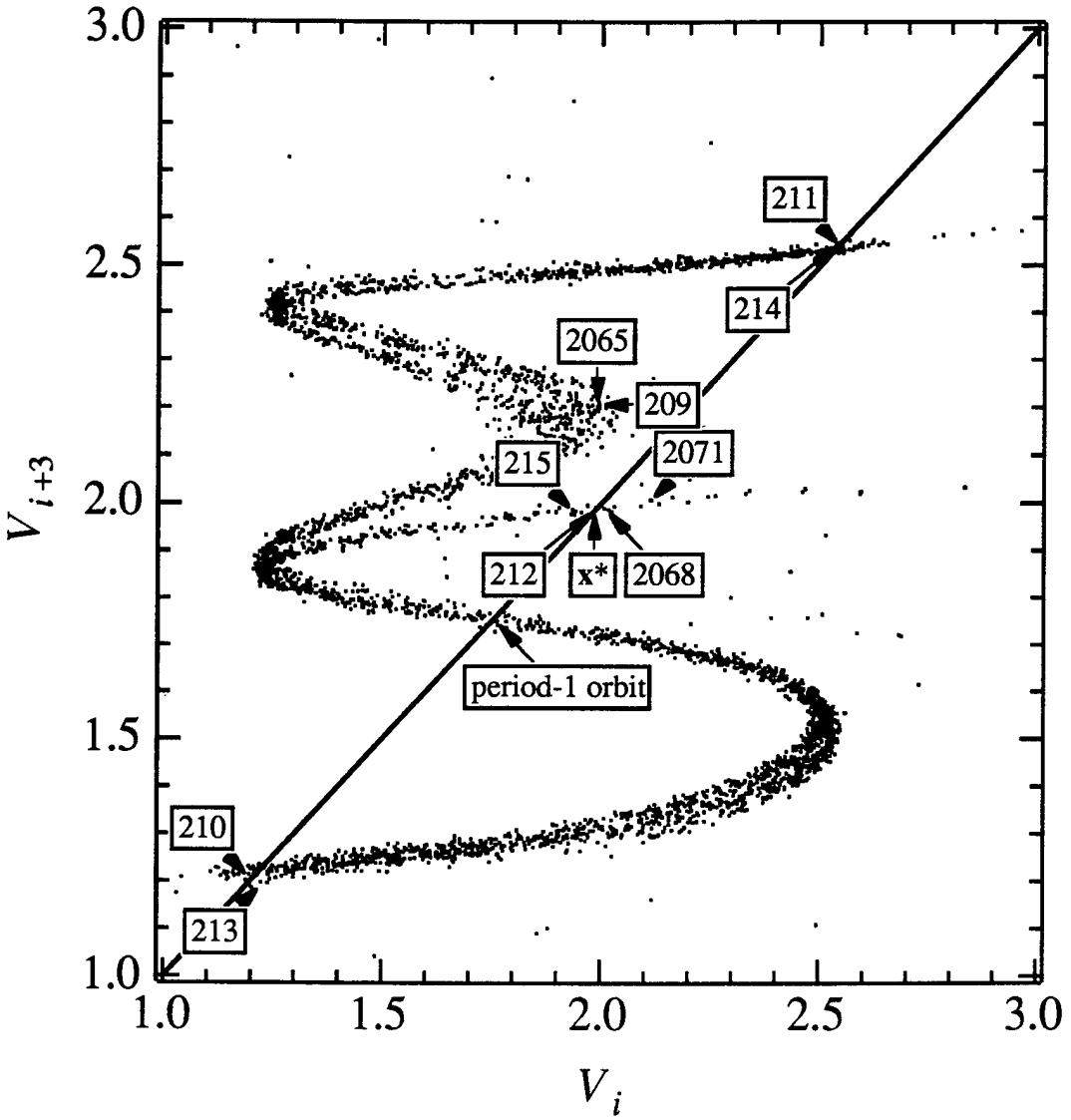

FIG. 24. Delay-coordinate embedding of time series taken after crisis. The boxed numbers indicate the iterate number *i*.

C. Analysis of Noise-induced Crisis

Although the analysis in the previous section was carried out as though the system operated with $a_k \equiv 0$ were deterministic, even then there is some residual noise in the system, resulting from mechanical vibrations and imperfections in the operational amplifier. This residual system noise must be taken into account when applying Eq. (2), in which the strength σ of the *total* noise experienced by the system appears. We allowed for this fact as follows. When the system was operated at a different set of parameters ($H_{dc} = 0.22$ Oe, $H_{ac} = 2.05$ Oe, f=0.95 Hz) it was noted that the attractor was not chaotic, but rather was a *stable* periodic orbit. The sequence of iterates V_i had a Gaussian distribution, due to the system noise, with a standard deviation σ_V of about 5mV. As the variable noise was increased, the distribution remained gaussian, but broadened. As shown in Fig. 25 the effect of the variable noise on the system state was well described by an additive variance model, consistent with the residual system noise and the variable noise being independent Gaussian processes. In testing the applicability of Eq. (2), we used an effective noise strength $\sigma = [\sigma_0^2 + \sigma_a^2]^{1/2}$,where σ_0, the residual system noise, was determined from the fit in Fig. 25.

Figure 26(a) shows the characteristic times $\hat{\tau}$ estimated from data runs taken at a wide variety of noise and (pre-crisis, $f > f_c$) parameter values. In Fig. 26(b), the scaling indicated by Eq. (2) has been applied, using the critical exponent determined for $f < f_c$ and $a_k \equiv 0$. The widely dispersed data of Fig. 26(a) now collapse to a single curve, which gives the graph of the function $g(\bullet)$ in Eq. (2) for this system. This consistency strongly supports the theory underlying scaling law (2).

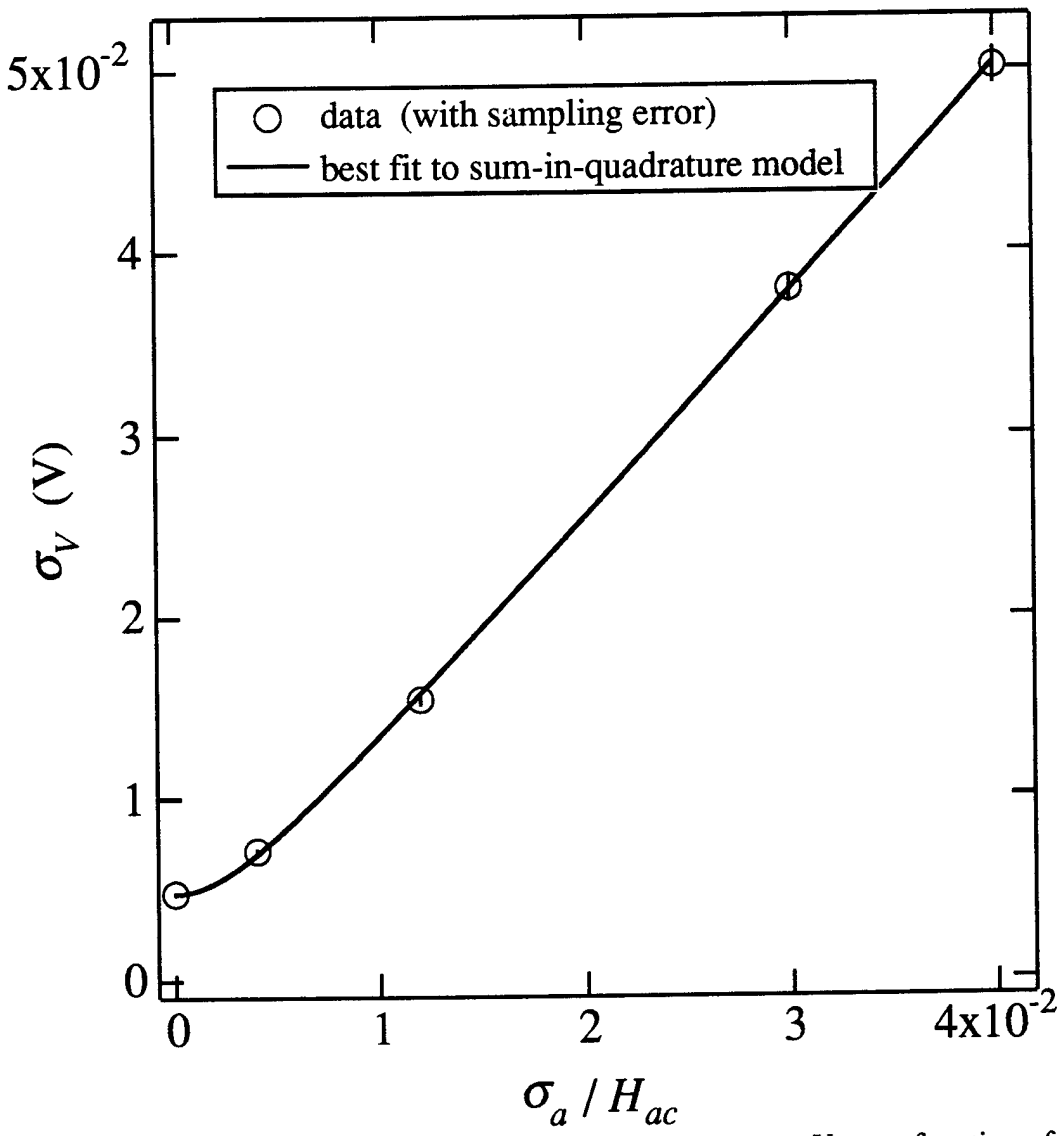

FIG. 25. Measured standard deviation of the iterate sequence V_i, as a function of the strength of the added noise. Here, the system's attractor is a stable periodic orbit. The curve shows the best fit to the sum-in-quadrature model $\sigma_V = k[\sigma_0^2 + \sigma_a^2]^{1/2}$.

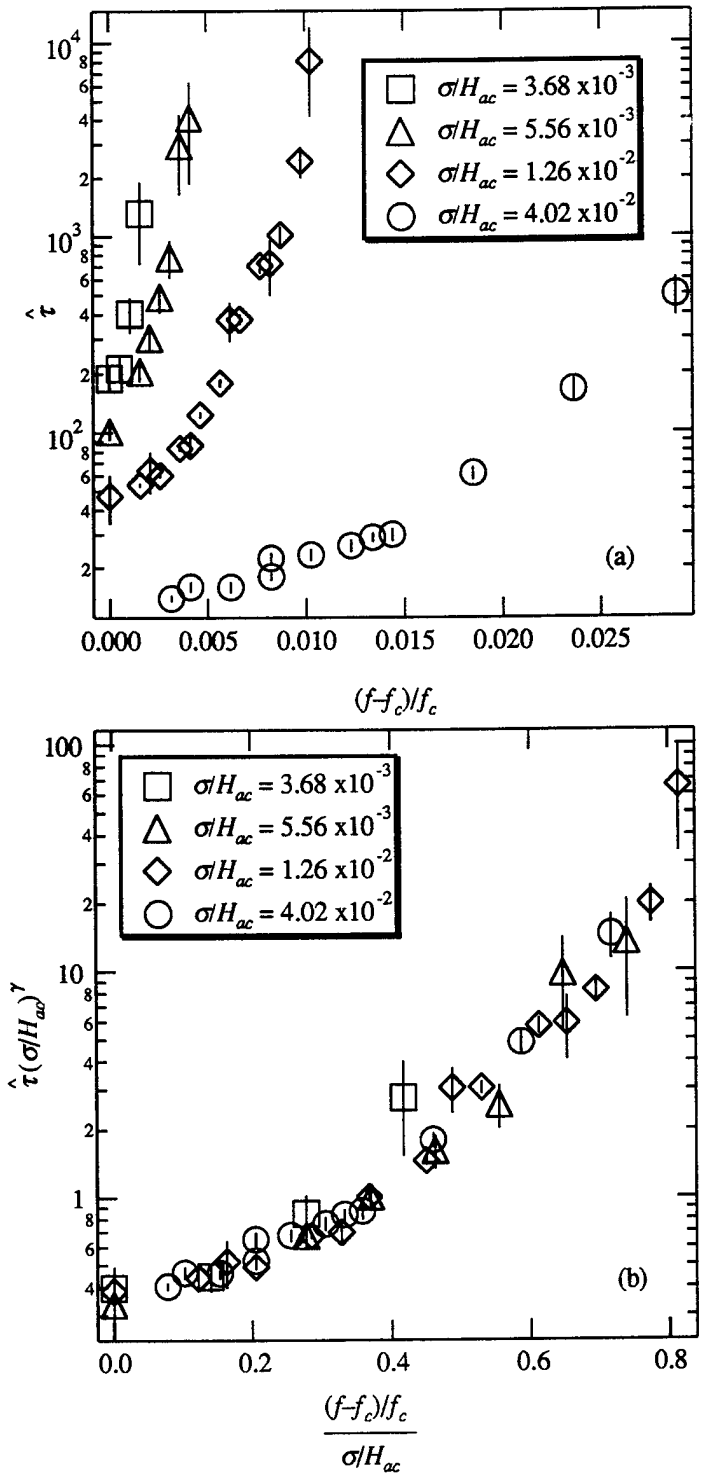

FIG. 26. Characteristic times for noise-induced bursting. (a) shows range of raw data. Scaling of Eq. (2) is applied in (b), using deterministic critical exponent γ. Data collapse onto a single curve, giving graph of function $g(\bullet)$ in Eq. (2).

IX. CONCLUSIONS

In this dissertation we have introduced a general scaling law for the characteristic time τ of noisy systems operating at parameter values near those corresponding to a deterministic crisis. The scaling law (2), applicable to systems whose deterministic crises are governed by the scaling law (1), shows that, although the strength of noise in the system is fundamental in determining the characteristic time τ, the noise-induced crisis inherits its governing exponent γ from the deterministic system. For the case of the noisy logistic map, our results reduce to a previously known special case.[9]

Numerical examples suggest that the noise scaling law can be expected to apply to crises resulting in attractor destruction, attractor enlargement, and attractor merging, for both maps and flows. However, some complications to the observability of the scaling law have also been identified.

A physical experiment further supports the theory underlying scaling laws (1) and (2). The fact that the noise in the experiment appeared *parametrically* shows that the applicability of Eq. (2) is even wider than suggested by the numerical results.

The ubiquity of noise in physical systems means that the experimental investigation of systems near crisis should be done with congnizance of scaling law (2). Conversely, the inheritance of the critical exponent from the deterministic crisis by the noise-induced crisis means that the intentional addition of noise may be an important experimental probe for investigating the deterministic dynamics underlying a noise-limited system.

APPENDIX A: DERIVATION OF EQS. (12) AND (13)

In this appendix we derive the first-order correction terms to the overall rate of escape for orbits of the noisy logistic map, Eqs. (12) and (13). The left-hand escape rate L is derived by first considering the dynamical density $P_{X+Z}(w)$ of orbits near the right edge of the attractor, after noise has been added, but before the deterministic part of the map has again been applied:

$$P_{X+Z}(w) = \int_{-\infty}^{\infty} \rho(x)\, P_Z(w-x)\, dx$$

$$= \int_{-\infty}^{p/4} \frac{1}{\pi\sqrt{p/4-x}} \; \frac{1}{\sigma\sqrt{2\pi}} exp[-(w-x)^2/2\sigma^2]\, dx.$$

Making the substitutions $s = w-p/4$ and $u = p/4-x$, we have

$$P_{X+Z}(s) = \frac{1}{\pi^{3/2}\,\sigma\sqrt{2}} exp(-s^2/2\sigma^2) \int_0^{\infty} u^{-1/2} exp\left(\frac{u^2}{2\sigma^2} - \frac{s}{\sigma^2}\right) du,$$

and using an integral definition of the parabolic cylinder function [see Ref. 20, Eq. 3.462 (1)] , we get

$$P_{X+Z}(s) = \frac{1}{\pi^{3/2}\,\sigma\sqrt{2}} exp(-s^2/4\sigma^2)\, D_{-1/2}(s/\sigma).$$

The integral of this result over $[1,\infty)$ yields the right-hand escape rate R. By applying the deterministic part of the map (12), one obtains the density of orbits near the left side of the attractor, before the noise kick:

$$\tilde{P}_{X+Z}(x) = \frac{1}{\pi^{3/2}\,4\sigma\sqrt{2}} exp[-(1-p/4-x/4)^2/4\sigma^2]$$

$$\times D_{-1/2}[(1-p/4-x/4)/\sigma].$$

The density of orbits after the noise is added is obtained by convolving the noise density with the part of $\tilde{P}_{X+Z}(x)$ to the right of x=0. The integral of the resulting convolution gives the left-hand escape rate L. Because the convolution does not exist in

closed form, we use a polynomial approximation to $\tilde{P}_{X+Z}(x)$ in the neighborhood of $x=0$ (we use an asymptotic expansion):

$$\tilde{P}_{X+Z}(x) \approx \sum_{k=0}^{k_{max}} \tilde{P}^{(k)}_{X+Z}(0) \frac{x^k}{k!}.$$

Now the convolution integral can be evaluated:

$$L = \int_{-\infty}^{0} dy \int_{0}^{\infty} dx \sum_{k=0}^{k_{max}} \tilde{P}^{(k)}_{X+Z}(0) \frac{x^k}{k!} P_Z(y-x),$$

or, substituting $u=y-x$, we have

$$= \int_{-\infty}^{0} dy \int_{-\infty}^{y} du \sum_{k=0}^{k_{max}} \tilde{P}^{(k)}_{X+Z}(0) \frac{(y-u)^k}{k!} P_Z(u).$$

Reversing the order of the sum over k and the integrations, expanding the binomial, integrating by parts, and letting $w=-y$, we have

$$L = \sum_{k=0}^{k_{max}} \frac{\tilde{P}^{(k)}_{X+Z}(0)}{k!} \sum_{j=0}^{k} \binom{k}{j} (-1)^j \int_{-\infty}^{0} dy\, y^{k-j} \int_{-\infty}^{y} du\, u^j P_Z(u).$$

$$= \sum_{k=0}^{k_{max}} \frac{\tilde{P}^{(k)}_{X+Z}(0)}{k!} \sum_{j=0}^{k} \binom{k}{j} (-1)^{j+1} \frac{1}{k-j+1} \int_{-\infty}^{0} dy\, y^{k-j+1} y^j P_Z(y)$$

$$= \sum_{k=0}^{k_{max}} \frac{\tilde{P}^{(k)}_{X+Z}(0)}{k!} \sum_{j=0}^{k} \binom{k}{j} (-1)^{j+k} \frac{1}{k-j+1} \times \int_{0}^{\infty} dw\, w^{k+1} \frac{1}{\sigma\sqrt{2\pi}} exp(-w^2/2\sigma^2).$$

Using the definition of the gamma function, we have

$$L = \sum_{k=0}^{k_{max}} \frac{\tilde{P}^{(k)}_{X+Z}(0)}{k!} (-1)^k \frac{\sigma^{k+1} 2^{(k-1)/2}}{\pi^{1/2}} \Gamma(k/2+1)$$

$$\times \sum_{j=0}^{k} \binom{k}{j} (-1)^{j+k} \frac{1}{k-j+1}.$$

The sum over j can be simplified, yielding

$$L = \sum_{k=0}^{k_{max}} \frac{\tilde{P}^{(k)}_{X+Z}(0)}{k!} (-1)^k \frac{\sigma^{k+1} 2^{(k-1)/2}}{\pi^{1/2}} \Gamma(k/2+1)\, (-1)^k \frac{1}{k+1}$$

$$= \sum_{k=0}^{k_{max}} \frac{\tilde{P}^{(k)}_{X+Z}(0)}{(k+1)k!} \frac{\sigma^{k+1} 2^{(k-1)/2}}{\pi^{1/2}} \Gamma(k/2+1).$$

Finally, we use the following recursion relation for the parabolic cylinder functions,

$$\frac{\partial}{\partial x} D_k(x) = \frac{x}{2} D_k(x) - D_{k+1}(x),$$

(see Ref. 12, Eq. 19.6.2) to find the derivative

$$\tilde{P}^{(k)}_{X+Z}(x) = \frac{1}{4^{k+1} \pi \sigma^{k+1/2} \sqrt{2}} exp[-(1-p/4-x/4)^2/4\sigma^2]$$

$$\times D_{k-1/2}[(1-p/4-x/4)/\sigma],$$

yielding

$$L = \frac{\sigma^{1/2}}{8\pi^{3/2}} exp\left[-\frac{(1-p/4)^2}{4\sigma^2}\right] \sum_{k=0}^{k_{max}} \frac{\Gamma(k/2+1)}{(k+1)\, k!\, 2^{3k/2}} D_{k-1/2}[(1-p/4)/\sigma] .$$

Using the fact that for the logistic map p_c=4, we obtain Eq. (12).

The steps in deriving $\overline{R}$, the failure rate for right-hand escapes, are exactly the same, except the limits of integration are permuted:

$$\overline{R} = \int_0^{\infty} dy \int_{-\infty}^{0} dx \sum_{k=0}^{k_{max}} \tilde{P}^{(k)}_{X+Z}(0) \frac{x^k}{k!} P_Z(y-x) .$$

The result is the same as for L, except that the series is an alternating one, yielding Eq. (13).

APPENDIX B: INTEGRATION OF STOCHASTIC DIFFERENTIAL EQUATIONS

Obtaining realizations of stochastic differential systems such as Eq. (17) is a less well-developed branch of numerical analysis than the numerical solution of ordinary differential equations. Various *ad hoc* schemes have appeared in the literature (cf. Refs. 8 and 9) that undoubtedly provide qualitatively correct results, but which may not be accurate enough when numerical results are to be compared with experimental results, or, as discussed below, with numerical results for the corresponding deterministic system. For the results presented in Chapter VI, we used a one-step colocation integration scheme closely related to that reported in Ref. 21. The idea of the method is to use a single pseudorandom vector to account for the cumulative effect of the stochastic process $\xi(t)$ over the whole integration time step, respecting the influence of the dynamics on the noise-perturbed orbit throughout the time step.

The method we used has an associated single-step error which is $o(\Delta t^{5/2})$ in the integration time step Δt. This is much larger than the single-step error associated with most numerical methods widely used to solve deterministic ODEs. The characteristic behavior of random walks (displacement~$\Delta t^{1/2}$) means that, for the n^{th} level of successive approximation in the numerical method, the error terms are $o(\Delta t^{n/2})$. Unfortunately, the complexity of the the stochastic integrals arising in the numerical method becomes prohibitive very quickly, and errors of order $o(\Delta t^{5/2})$ are all that have ever been used in practice. Further, the use of adaptive step-size control in a stochastic integrator is very difficult (and no such algorithms have been published).

The problem caused by the large error is manifested when simulated stochastic results are to be compared to numerical results from the corresponding deterministic system. A numerical integration scheme is really a discrete map, where one of the parameters is the integration time step. Thus even a deterministic system,

integrated by two different schemes, or by the same scheme using two different time steps, may well produce different results. In particular, the parameter values at which crises occur are likely to vary, depending on the integration scheme. In order to avoid any such problems with our comparisons of the deterministic and noisy Duffing oscillators, we integrated the deterministic system using the exact same algorithm and time step as for the noisy system, but omitting the noise terms. The resulting second-order Euler algorithm yielded numerical results that differed slightly from those previously reported[5] for the deterministic version of Eq. (17).

APPENDIX C: ESTIMATION OF EIGENVALUES OF UNSTABLE SADDLES FROM EXPERIMENTAL DATA

Our general eigenvalue estimation procedure is outlined as follows. To obtain the eigenvalues of a period-n orbit, we approximate the map $\mathbf{F}^{(n)}$ (the n-times-iterated map $\mathbf{F}$) by a Taylor series

$$\mathbf{x}_{i+n} + \delta\mathbf{x}_{i+n} = \mathbf{F}^{(n)}(\mathbf{x}_i) + \mathbf{DF}^{(n)}\big|_{\mathbf{x}_i} \cdot \delta\mathbf{x}_i + O(|\delta\mathbf{x}_i|^2),$$

and let $\mathbf{x}_i$ be the period-n point, which we denote $\mathbf{x}^*$. Because $\mathbf{F}^{(n)}(\mathbf{x}^*)=\mathbf{x}^*$, we see that the Jacobian $\mathbf{DF}^{(n)}\big|_{\mathbf{x}^*}$ takes tangent vectors into tangent vectors near the saddle. We can use the difference between a pair of iterates on the same orbit to approximate a tangent vector, and watch its propagation near the period-n point:

$$\mathbf{x}_{i+n} - \mathbf{x}_{j+n} \approx \mathbf{DF}^{(n)}\big|_{\mathbf{x}^*} \cdot (\mathbf{x}_i - \mathbf{x}_j), \quad i \neq j.$$

The key advantage of this method over that of Ref. 5 (1987) is that here we can take advantage of widely (temporally) separated recurrent iterates (*i.e.*, i very different from j). Furthermore we do not require many sequential iterates which are all within the linear neighborhood of the saddle and whose differences are also significantly above the system noise level.

Because we use a delay-coordinate embedding, the surface of section map for $\mathbf{x}=(y,z)$ is of the form

$$\begin{cases} y_{i+n} = h(y_i, z_i) \\ z_{i+n} = y_i \end{cases},$$

and we therefore know that the form of the Jacobian is particularly simple:

$$\mathbf{DF}^{(n)}\big|_{\mathbf{x}^*} = \begin{pmatrix} r & s \\ 1 & 0 \end{pmatrix},$$

where $r=\partial h/\partial y\big|_{(y^*,\, z^*)}$ and $s=\partial h/\partial z\big|_{(y^*,\, z^*)}$.

Calculating the eigenvalues of $\mathbf{DF}^{(n)}\big|_{\mathbf{x}^*}$ explicitly and using Eq. (5) and the fact that $\beta_1\beta_2 = \det\left(\mathbf{DF}^{(n)}\big|_{\mathbf{x}^*}\right)$, we have $\gamma = \log[r/2 - \frac{1}{2}(r^2 + 4s)^{1/2}]/[2\log|s|)]$. Thus,

estimation of the eigenvalues of the period-n orbit is reduced to the statistical estimation of the quantities r and s, from the linear multiple regression model

$$y_{i+n} - y_{j+n} = r\,(y_i - y_j) + s\,(z_i - z_j)\,,$$

where a set of $(i \neq j)$ pairs is chosen from the vicinity of the saddle. Constraints can be placed on the regression, because the sign of s will be known from the type of period-n saddle involved (an ordinary saddle implies $s<0$; a flip saddle implies $s>0$). Furthermore, the $(i \neq j)$ pairs can be chosen in such a way as to maximize the statistical confidence of the estimates, *i.e.*, chosen such that the contributions of the r and s terms in the regression are about equal. [Use of the restricted form of the Jacobian and a careful choice of data for the regression analysis is essential in a noisy system. Least-squares estimation of the general Jacobian with a comprehensive data set was done successfully with a lower-noise system in Ref. 22, but for our system, this results in a very poor estimate of the stable eigenvalue, and consequently, a poor estimate of γ.] Finally, propagation of errors using the $\gamma(r,s)$ formula allows the statistical uncertainties in r and s to be translated into uncertainty in γ. A nearly identical analysis pertains to the heteroclinic case.

For the particular crisis of interest in Chapter VIII, we take the point x* to be as shown in Fig. 4. Observation of iterates passing near x* shows that the period-3 saddle is an ordinary one ($s<0$), that the stable direction is nearly vertical , and that the unstable direction has a slope of about 0.1. The second row of **DF** indicates that the eigenvectors must be of the form $(\beta,1)$. We therefore know that $\beta_2 \ll 1$, while $\beta_1 \approx 10$, indicating that $|s| \ll |r|$, i.e., **DF** is ill-conditioned. This information allows the determination that the best regression estimates of r and s will be obtained for pairs of iterates whose vector difference is nearly vertical. Using 150 such pairs from a single orbit, we estimated r, s and their statistical uncertainties, and conclude that $\gamma = 1.07 \pm 0.15$.

REFERENCES

[1]C. Grebogi, E. Ott, and J. A. Yorke, Phys. Rev. Lett. **48,** 1507 (1982); C. Grebogi, E. Ott, and J. A. Yorke, Physica (Amsterdam) **7D**, 181 (1983).

[2]C. Jeffries and J. Perez, Phys. Rev. A **27**, 601 (1983); S. K. Brorson, D. Dewey, P. S. Linsay, *ibid.* **28**, 1201 (1983); H. Ikezi, J. S. deGrasse, and T. H. Jensen, *ibid.* **28**,1207 (1983); R. W. Rollins and E. R. Hunt, *ibid.* **29**, 3327 (1984); E. G. Gwinn and R. M. Westervelt, Phys. Rev. Lett. **54**, 1613 (1985); D. Dangoisse, P. Glorieux, and D. Hannequin, *ibid.* **55**, 746 (1985).

[3]T. L. Carroll, L. M. Pecora and F. J. Rachford, Phys. Rev. Lett. **59**, 2891 (1987); W. L. Ditto, *et al. ibid.* **63**, 923 (1989).

[4]J. A. Yorke and E. D. Yorke, J. Stat. Phys. **21**, 263 (1979).

[5]C. Grebogi, E. Ott, and J. A . Yorke, Phys. Rev. Lett. **57**, 1284 (1986); C. Grebogi, E. Ott, F. Romeiras, and J. A . Yorke, Phys. Rev. A **36**, 5365 (1987).

[6]see for example, the bibliography in R. Landauer, *Noise-activated escape from metastable states: an historical view*, in *Noise in Nonlinear Dynamical Systems*, vol. 1, F. Moss and P. V. E. McClintock, eds., Cambridge (1989).

[7]J. Crutchfield, M. Nauenburg and J. Rudnick, Phys. Rev. Lett. 4**6,** 933 (1981); B. Schraiman, C. E. Wayne and P.C. Martin, *ibid.* **46**, 935 (1981). J. G. Hirsch, M. Nauenberg and D. J. Scalapino, Phys. Lett. **87A**,391 (1982).

[8]R. Kapral, M. Schell, and S. Fraser, J. Phys. Chem. **86**, 2205 (1982); R. L. Kautz, J. Appl. Phys. **62**, 198 (1987); P. D. Beale, Phys. Rev. A **40**,3998 (1989).

[9]F. T. Arecchi, R. Badii, and A. Politi. Phys. Lett. **103A**, 3 (1984).

[10]E. Ott, W. D. Withers, and J. A. Yorke, J. Stat. Phys. **36**, 243 (1984).

[11]P. Collet and J. P. Eckmann, *Iterated Maps on the Interval as Dynamical Systems*, Birkhäuser (1980).

[12]M. Abramovitz and I. A. Stegun, *Handbook of Mathematical Functions*, § 19.5, Dover (1972).

[13]S. M. Hammel, C. K. R. T. Jones, and J. V. Moloney, J. Opt. Soc. Am. B **2**, 552 (1985).

[14]L. J. Bain, *Statistical Analysis of Reliability and Life-testing Models*, Ch. 3, Marcel Dekker, Inc., New York (1978).

[15]H. Ishii, H. Fujisaka, and M. Inoue, Phys. Lett. **116A,** 257 (1986).

[16]H. T. Savage and C. Adler, J. Magn. Magn. Mater. **58**, 320 (1986); H. T. Savage and M. L. Spano, J. Appl. Phys. **53**, 8002 (1982).

[17]H. T. Savage, *et al.*, J. Appl. Phys. **67**, 5619 (1990).

[18]F. Takens, in *Dynamical Systems and Turbulence*, edited by D. A. Rand and L.-S. Young (Springer-Verlag, Berlin, 1980), pp. 366ff; N. H. Packard *et al.*, Phys. Rev. Lett. **45**, 712 (1980).

[19]W. L. Ditto, S. N. Rauseo and M. L. Spano, Phys. Rev. Lett. **63**, 3211(1989); W. L. Ditto, *et al.*, *ibid.* **65**, 533 (1990).

[20]I. S. Gradshteyn and I. M. Ryzhik, *Table of Integrals, Series, and Products*, Academic Press (1980).

[21]N. J. Rao, J. D.Borwankar, and D. Ramkrishna, SIAM J. Control **12**, 124 (1974); the method is explained at greater length in R. Mannella, *Computer experiments in nonlinear stochastic physics*, in *Noise in Nonlinear Dynamical Systems*, vol. 3, F. Moss and P.V.E. McClintock, eds., Cambridge (1989). Fortunately, for simple additive coupling of the noise as in Eq. (17), the Stratonovich and Ito interpretations of the stochastic differential equation result in the same numerical algorithm, so we leave no practical ambiguity by not discussing this issue.

[22]D. P. Lathrop and E. J. Kostelich, Phys. Rev. A **40**, 4028 (1989).